Title

Influence of Self-MHC Class I Recognition on the Dynamics of NK Cell Responses to Cytomegalovirus Infection.

Journal

The Journal of Immunology, 208(7)

ISSN

0022-1767

Authors

Potempa, Marc
Aguilar, Oscar A
Gonzalez-Hinojosa, Maria DR
et al.

Publication Date

2022-04-01

DOI

10.4049/jimmunol.2100768

Peer reviewed

The Journal of Immunology

Influence of Self–MHC Class I Recognition on the Dynamics of NK Cell Responses to Cytomegalovirus Infection

Marc Potempa, Oscar A. Aguilar, Maria D. R. Gonzalez-Hinojosa, Iliana Tenvooren, Diana M. Marquez, Matthew H. Spitzer and Lewis L. Lanier

J Immunol published online 23 March 2022
http://www.jimmunol.org/content/early/2022/03/23/jimmunol.2100768

Supplementary Material **http://www.jimmunol.org/content/suppl/2022/03/23/jimmunol.2100768.DCSupplemental**

The Journal of Immunology is published twice each month by
The American Association of Immunologists, Inc.,
1451 Rockville Pike, Suite 650, Rockville, MD 20852

Print ISSN: 0022-1767 Online ISSN: 1550-6606.

Published March 23, 2022, doi:10.4049/jimmunol.2100768

Influence of Self–MHC Class I Recognition on the Dynamics of NK Cell Responses to Cytomegalovirus Infection

Marc Potempa,* Oscar A. Aguilar,*,† Maria D. R. Gonzalez-Hinojosa,*,† Iliana Tenvooren,*,†,‡,§,¶ Diana M. Marquez,*,†,‡,§,¶ Matthew H. Spitzer,*,†,‡,§,¶ and Lewis L. Lanier*,†

Although interactions between inhibitory Ly49 receptors and their self–MHC class I ligands in C57BL/6 mice are known to limit NK cell proliferation during mouse CMV (MCMV) infection, we created a 36-marker mass cytometry (CyTOF) panel to investigate how these inhibitory receptors impact the NK cell response to MCMV in other phenotypically measurable ways. More than two thirds of licensed NK cells (i.e., those expressing Ly49C, Ly49I, or both) in uninfected mice had already differentiated into NK cells with phenotypes indicative of Ag encounter (KLRG1$^+$Ly6C$^-$) or memory-like status (KLRG1$^+$Ly6C$^+$). These pre-existing KLRG1$^+$Ly6C$^+$ NK cells resembled known Ag-specific memory NK cell populations in being less responsive to IL-18 and IFN-α stimulation in vitro and by selecting for NK cell clones with elevated expression of a Ly49 receptor. During MCMV infection, the significant differences between licensed and unlicensed (Ly49C$^-$Ly49I$^-$) NK cells disappeared within both CMV-specific (Ly49H$^+$) and nonspecific (Ly49H$^-$) responses. This lack of heterogeneity carried into the memory phase, with only a difference in CD16 expression manifesting between licensed and unlicensed MCMV-specific memory NK cell populations. Our results suggest that restricting proliferation is the predominant effect licensing has on the NK cell population during MCMV infection, but the inhibitory Ly49–MHC interactions that take place ahead of infection contribute to their limited expansion by shrinking the pool of licensed NK cells capable of robustly responding to new challenges. *The Journal of Immunology*, **2022, 208: 1–13.**

Natural killer cells monitor other cells for signs of infection or tumorigenesis and eliminate them when identified (1). They accomplish this surveillance through two complementary methodologies: positive recognition of stress ligands, viral proteins, Ab-opsonized cells, or other "nonself" molecules by stimulatory and costimulatory receptors (2) and by a "missing-self" mechanism in which inhibitory NK cell receptors (NKRs) are no longer engaged due to the downregulation of MHC class I (MHC-I) molecules on unhealthy cells (3). Not all NK cells are equally capable of both strategies, however. Many NKRs, such as those of the Ly49 receptor family in mice and killer cell Ig-like receptor family in humans, are not guaranteed to be on every NK cell, but instead depend upon a semistochastic process during development for expression (4–6). That randomness is further complicated by allelic polymorphisms (7), epigenetic factors (8–10), and environmental conditions (11–13). The end result is a pool of cells comprising almost any given combination of activating and inhibitory NKRs with variegated expression levels of those NKRs. That means some proportion of mature NK cells will lack inhibitory receptors capable of recognizing the MHC-I alleles expressed within the same organism. Such "unlicensed" NK cells at steady state are unprepared to perform missing-self recognition and are additionally hyporesponsive to activating stimuli in vitro due to a lack of "education" through those inhibitory NKR–MHC interactions (14–16).

Nevertheless, if unlicensed cells are exposed to proinflammatory cytokines, they become as responsive to stimulatory ligands as their licensed NK cell counterparts (i.e., the NK cells expressing inhibitory NKRs engaging self–MHC-I ligands) (14, 15, 17). The unlicensed NK cells may even be at an advantage after cytokine stimulation due to the lack of a concurrent and dominant inhibitory signal (17–19). A clear example of when unlicensed cells are at an advantage is during mouse CMV (MCMV) infection of C57BL/6 (B6) mice. Proliferation of NK cells expressing Ly49C and/or Ly49I, which are the NKRs responsible for licensing in B6 mice, is dramatically limited in comparison with unlicensed cells, ultimately making licensed cells less protective (17). This restriction results from the recruitment of the phosphatase Src homology region 2 domain-containing phosphatase 1 (SHP-1) to the immunological synapse via the ITIMs in the cytoplasmic domains of these receptors (20, 21). SHP-1 then dephosphorylates Vav-1 (2, 18), a guanine nucleotide exchange factor and adaptor molecule with a key role in promoting lymphocyte proliferation (22).

*Department of Microbiology and Immunology, University of California, San Francisco, San Francisco, CA; †The Parker Institute for Cancer Immunotherapy, San Francisco, CA; ‡Department of Otolaryngology–Head and Neck Surgery, University of California, San Francisco, San Francisco, CA; §Helen Diller Family Comprehensive Cancer Center, University of California, San Francisco, San Francisco, CA; and ¶Chan Zuckerberg Biohub, San Francisco, CA

ORCIDs: 0000-0003-3853-3948 (M.P.); 0000-0002-7990-8745 (O.A.A.); 0000-0002-9833-7669 (I.T.); 0000-0001-5343-8696 (D.M.M.); 0000-0002-5291-3819 (M.H.S.); 0000-0003-1308-3952 (L.L.L.).

Received for publication August 4, 2021. Accepted for publication January 18, 2022.

This work was supported by the Parnassus Flow Cytometry Core (RRID:SCR_018206) supported in part by National Institutes of Health (NIH) Grant P30 DK063720 and Office of Extramural Research, NIH S10 Instrumentation Grant S10 1S10OD018040-01. O.A.A. holds a Postdoctoral Enrichment Program Award from the Burroughs Wellcome Fund and is a Cancer Research Institute Irvington Fellow supported by the Cancer Research Institute. O.A.A., M.D.R.G.-H., and L.L.L. are supported by the Parker Institute for Cancer Immunotherapy and Office of Extramural Research, NIH Grants R01 AI068129 and AI146581.

Lewis L. Lanier is a Distinguished Fellow of AAI.

Address correspondence and reprint requests to Dr. Lewis L. Lanier, Department of Microbiology and Immunology, University of California, San Francisco, 513 Parnassus Avenue, HSE 1001G, Box 0414, San Francisco, CA 94143-0414. E-mail address: lewis.lanier@ucsf.edu

The online version of this article contains supplemental material.

Abbreviations used in this article: B6, C57BL/6; DPI, day postinfection; ILC, innate lymphoid cell; MCMV, mouse CMV; MHC-I, MHC class I; mNK, memory NK; MSI, mean signal intensity; NKR, NK cell receptor; PCA, principal component analysis; pemNK, pre-existing memory-like NK; PFA, paraformaldehyde; SHP-1, Src homology region 2 domain-containing phosphatase 1; UCSF, University of California San Francisco.

The activities of Vav1 in NK cell function are multifaceted (23–25); however, whether the impact of licensing on the NK cell response under inflammatory conditions extends beyond proliferation has not been investigated. In pursuit of this aim, we constructed a 36-marker mass cytometry immunophenotyping panel for the analysis of group 1 innate lymphoid cells (ILCs) and applied it to the model of MCMV infection of B6 mice. As prefaced, these mice express the inhibitory Ly49C and/or Ly49I receptors on a subset of their NK cells, and those cells are then educated through their interactions with the MHC-I H2-K^b allele (26). B6 mice also express the activating NKR Ly49H, a receptor that enables the direct identification and killing of MCMV-infected cells via recognition of the viral glycoprotein m157 (27, 28). Thus, four critical populations are present within B6 mice: licensed and unlicensed versions of both m157 Ag-specific and Ag nonspecific NK cells. The Ag-specific response additionally results in the formation of an NK cell memory population (29), ultimately allowing us to phenotypically compare licensed and unlicensed cells not only during the expansion and contraction phases, but also in the memory phase of an immune response.

Materials and Methods

Animals

B6 mice were purchased from the National Cancer Institute at 6 wk of age and housed in the specific pathogen-free animal facility at the University of California, San Francisco (UCSF) thereafter, in accordance with the guidelines of the Institutional Animal Care and Use Committee. *Klra8*$^{-/-}$ (Ly49H-deficient) B6 mice were bred and maintained in the same facility. Germ-free B6 mice were bred and maintained within the UCSF Gnotobiotic Core. Experiments used mice of both sexes, aged 8–12 wk.

MCMV infection

Wild-type B6 mice were infected with 1000 PFUs of Smith strain MCMV via i.p. injection. Ly49H-deficient mice received 1 PFU. PBMCs were acquired at 7 d postinfection (DPI) from mice in the 14, 28, and 35 DPI groups and examined by flow cytometry. Infection status of these animals was confirmed via the observation of KLRG1 upregulation on NK cells and $CD8^+$ T cells.

Mass cytometry Abs

All were commercially available except for the anti–NKR-P1B Ab clone 2D12, which was generously provided by Iizuka et al. (30). Of note, the 5E6 Ab used to differentiate licensed and unlicensed NK cells binds to both Ly49C and Ly49I but is limited in its ability to detect $Ly49C^+Ly49I^-$ cells in B6 mice due to epitope masking via *cis* interactions with MHC-I molecules (31). The Abs used were: 2B4 (m2B4, #133501, BioLegend; panel 1: Sm147, panel 2: Sm147), CD2 (RM2-5, #100102, BioLegend; panel 1: Dy164, panel 2: Dy164), CD3 (17A2, #100202, BioLegend; panel 1: Gd157, panel 2: Gd157), CD8 (53-6.7, #100702, BioLegend; panel 1: Gd155, panel 2: Gd155), CD11a (M17/4, #101101, BioLegend; panel 1: Dy161, panel 2: not applicable), CD11b (M1/70, #101202, BioLegend; panel 1: In113, panel 2: Ho165), CD16 (AT154-2, #MCA5998, Bio-Rad Laboratories; panel 1: Nd144, panel 2: Nd144), CD19 (6D5, #115502, BioLegend; panel 1: Yb173, panel 2: Yb173), CD26 (H194-112, #137802, BioLegend; panel 1: not applicable, panel 2: Er167), CD27 (LG.3A10, #138302, BioLegend; panel 1: Ce140, panel 2: Bi209), CD32 (AT130-5, #MCA6000, Bio-Rad Laboratories; panel 1: Yb171, panel 2: Eu153), CD45 (30-F11, #103102, BioLegend; panel 1: In115, panel 2: In113), CD49b (DX5, #14-5971-85, Invitrogen; panel 1: Sm152, panel 2: Sm152), CD69 (H1.2F3, #104502, BioLegend; panel 1: Sm154, panel 2: Sm154), CD90 (30-H12, #105302, BioLegend; panel 1: Yb176, panel 2: Yb176), CD96 (3.3, #131704, BioLegend; panel 1: Nd146, panel 2: Nd146), CD127 (A7R34, #135002, BioLegend; panel 1: Nd150, panel 2: Nd150), CD132 (TUGm2, #132304, BioLegend; panel 1: Nd142, panel 2: Nd142), CD137 (17B5, #106114, BioLegend; panel 1: Er167, panel 2: Er166), CD200R1 (OX-110, #123902, BioLegend; panel 1: Ho165, panel 2: not applicable), CEACAM-1 (Mab-CC1, #134504, BioLegend; panel 1: Gd156, panel 2: Gd156), CXCR6 (SA051D1, #151102, BioLegend; panel 1: Er166, panel 2: not applicable), DNAM-1 (TX42.1, #133630, BioLegend; panel 1: Sm149, panel 2: Sm149), IFNAR (MAR1-5A3, #127302, BioLegend; panel 1: Nd148, panel 2: Nd148), IL-18Ra (A17071D, #157902, BioLegend; panel 1: Lu175, panel 2: Lu175, KLRG1 (2F1, #16-5893, Invitrogen; panel 1: Yb172, panel 2: Yb172), LAG-3 (C9B7W, #125202, BioLegend; panel 1: not applicable, panel 2: Yb171), Ly6C (HK1.4, #128002, BioLegend; panel 1: Eu151, panel 2: Pr141), Ly49A (YE1/48.10.6, #94015 [discontinued], BioLegend; panel 1: Dy163, panel 2: not applicable), Ly49C/I (5E6, #553273, BD Biosciences; panel 1: Bi209, panel 2: Er168), Ly49D (4E5, #138302, BioLegend; panel 1: La139, panel 2: Eu151), Ly49G2 (4D11, #555314, BD Biosciences; panel 1: Yb174, panel 2: Yb174), Ly49H (3D10, #144702, BioLegend; panel 1: Pr141, panel 2: Tb159), NK1.1 (PK136, #108702, BioLegend; panel 1: Gd160, panel 2: Gd160), NKG2ACE (20d5, #16-5896-85, Invitrogen; panel 1: Gd158, panel 2: Gd158), NKG2D (CX5, #130202, BioLegend; panel 1: Er170, panel 2: Er170), NKp46 (29A1.4, #137602, BioLegend; panel 1: Tm169, panel 2: Tm169), NKR-P1B (2D12; panel 1: Nd143, panel 2: Nd143), PD-1 (29F.1A12, #135202, BioLegend; panel 1: Tb159, panel 2: not applicable), and TIGIT (1G9, #142012, BioLegend; panel 1: not applicable, panel 2: Dy163).

Abs were conjugated to their associated metals with Maxpar X8 labeling reagent kits (DVS Sciences) according to the manufacturer's instructions, diluted with CANDOR PBS Ab Stabilization solution (CANDOR Bioscience) supplemented with 0.02% sodium azide, and filtered through an Ultrafree MC 0.1-μm centrifugation filter (Millipore) before storage at 4°C. Each metal-bound Ab was titrated on splenocytes collected from untreated wild-type B6 mice or B6 mice that received 150 μg of polyinosinic-polycytidylic acid via i.p. injection 18 h ahead of collection.

Sample preparation for mass cytometry

Spleens were mechanically dissociated using the flat end of the plunger from a 1-ml syringe and filtered through a 40-μm strainer. Following RBC lysis using ACK lysis buffer, cells were washed and resuspended in PBS with 5 mM EDTA (PBS/EDTA). The suspension was then mixed 1:1 with PBS/EDTA containing 100 mM cisplatin (Enzo Life Sciences) for viability staining. After 1 min, PBS with 5 mM EDTA plus 0.5% BSA (CyTOF Staining Media) was added at 1:1. Cells were washed, resuspended in CyTOF Staining Media, and counted.

One million splenocytes from each mouse were transferred into individual staining tubes and stained with metal-conjugated Abs against CD16 and CD32b for 15 min at room temperature in 100 μl volume. Following this initial incubation, an Fc blocking Ab (clone 2.4G2) was mixed into each stain and left for another 15 min at room temperature. Cells were washed twice before being stained with a master mix of all remaining metal-conjugated Abs for 30 min at room temperature in 100 μl volume.

For cells stained with the initial panel, following the Ab stain, cells were washed and then fixed for 10 min at room temperature using 1.6% paraformaldehyde (PFA) in PBS/EDTA. After another wash with PBS/EDTA, they were resuspended in PBS/EDTA with 10% DMSO and stored at −80°C for barcoding at a later date. Cells stained with the updated panel were not frozen, but instead were fixed and kept in 3.2% PFA in PBS/EDTA at 4°C for 3–5 d before proceeding to barcoding.

For barcoding, each sample was thawed, if necessary, washed once, and then resuspended in 1× Barcode Perm Buffer (Fluidigm). Splenocytes from each mouse were labeled with 1 of 20 distinct combinations of Pd isotopes, as described previously (32). When more than 20 mice were barcoded at once, as during the side-by-side infection of wild-type and Ly49H-deficient mice, samples from each genotype were split evenly between different sets of the barcode combinations. After washing in PBS/EDTA, all cells from each set of 20 barcodes were pooled. Pooled cells were then fixed in a 3.2% PFA in PBS/EDTA solution containing a 1:1000 dilution of a 191/193 Ir DNA intercalator (Fluidigm) and kept at 4°C overnight.

Mass cytometry data acquisition and normalization

Just prior to analysis, the barcoded samples were pelleted, washed in CyTOF Staining Media, washed twice more in double-deionized water, and then resuspended in double-deionized water containing a 1:20 dilution of EQ Four Element Calibration Beads (Fluidigm) at a concentration of ~10^6 cells/ml. The mixture was filtered through a 35-μm cell strainer and then analyzed on a CyTOF2-Helios mass cytometer (Fluidigm). The resulting data files were normalized using the mass cytometry data normalization algorithm (33), which uses the calibration beads to correct for inconsistencies in sample detection over time.

viSNE/FlowSOM plot generation

After normalization and debarcoding, live singlets were identified on the basis of DNA and a negative cisplatin stain. Group 1 ILCs were selected initially selected as $CD2^+CD3^-CD19^-2B4^+NK1.1^+$ before revising the phenotype to $CD2^+CD3^-CD8^-CD19^-2B4^+CEACAM\text{-}1^{lo/-}$ when splenocytes

from infected mice were included in the analysis. Example gating strategies can be found in Supplemental Fig. 1. FCS files containing the events isolated as group 1 ILCs were uploaded into the Web site–based Cytobank platform (34), and viSNE plots were generated there (35). All files were sampled equally, and all Ab-targeted markers were used for clustering unless otherwise noted. Where applicable, secondary analysis of the viSNE plots was done by FlowSOM (36). FlowSOM clustering was based solely on the tSNE1 and tSNE2 channels, and the hierarchical consensus clustering methodology was employed. The number of metaclusters and clusters was determined based on iterative testing.

Heat map generation

For heat maps representing FlowSOM metaclustering results, cluster medians and abundances data were downloaded from the Cytobank platform. Cluster medians were scaled within each channel as percentage of maximum and then grouped by metacluster. Values for each channel within a metacluster were then determined as the weighted average of the scaled cluster medians with weighting determined by cluster abundances. Heat maps were then generated in R (R Core Team, 2020) using the ComplexHeatmap package. The heat map in Fig. 6 was generated by manually gating the four Ly49I and Ly49H subsets with FlowJo software (Tree Star), exporting the event data for each group at each time point, and then proceeding to scale and average the data. To avoid the impact of outliers while scaling the data, the values used for scaling were the medians of the top 100 events within each channel. After generating the heat map in R, the columns were manually reorganized by time point and Ly49I and Ly49H subsets.

Principal component analysis and Euclidean distance calculations

Principal component analysis (PCA) was performed on data matrices using the basic Stats package in R. For the analysis in Fig. 1, the relevant matrix was that which was used to generate the heat map. For the infection data, Ly49I-positive and -negative subsets were manually gated in FlowJo with the additional separation into Ly49H-positive and -negative subsets if possible. Those data were exported, scaled within each channel as percent of maximum, and then averaged as for the Fig. 6 heat map. In each case, only two components explained more than 10% of the variance. For the calculation of similarity between $Ly49I^+$ and $Ly49I^-$ subsets, the Euclidean distance between all pairs of $Ly49I^+$ and $Ly49I^-$ cells, stratified by Ly49H, at each time point was determined.

Flow cytometry

Splenocytes from wild-type or infected mice were isolated by mechanical dissociation through a 0.4-μm cell strainer and freed from RBCs by treatment with ACK lysis buffer. Surface staining was performed using preconjugated Abs, and samples were run on an LSR II cytometer (BD Biosciences). The Abs used for flow cytometry were: CD2 (RM2-5, #100104; BioLegend), CD3ε (145-2C11, #100349 and #100330; BioLegend), CD8α (53-6.7, #612759; BD Biosciences), CD16 (S17014E, #158004; BioLegend), CD19 (6D5, #115534 and #115546; BioLegend), CD49b (DX5, #563063 and #108922; BD Biosciences), CD90.2 (30-H12, #105320; BioLegend), NK1.1 (PK136, #564144, BD Biosciences; #108739, BioLegend), 2B4 (m2B4 [B6]458.1, #133516; BioLegend), KLRG1 (2F1, #138429; BioLegend), Ly6C (HK1.4, #128049; BioLegend), Ly49C [4LO3311, a generous gift from Dr. Wayne Yokoyama (14)], Ly49H (3D10, #144710, BioLegend; and #744260, BD Biosciences), Ly49I (YLI-90, #11-5895-82; Thermo Fisher Scientific), FcεRIγ (polyclonal, #FCABS400F; EMD Millipore), and rabbit IgG isotype control (polyclonal, #11-4614-80; Invitrogen). An unconjugated anti-CD16/CD32 Ab (clone 2.4G2; UCSF Antibody Core Facility) was used to block nonspecific binding. In experiments measuring CD16 expression, cells were stained with the fluorophore-conjugated anti-CD16 Ab prior to treatment with 2.4G2, as the latter blocks binding of the CD16-specific Ab. An example gating strategy is presented in Supplemental Fig. 1. Data were analyzed in FlowJo.

In vitro stimulation assays

Splenocytes were harvested and processed into single-cell suspensions and RBC lysed. Cells were then stained for surface markers (NK1.1, NKp46, CD3ε, CD19, Ly6C, KLRG1, Ly49I, and Ly49H) and viability (Zombie Red; BioLegend), and then rested for 1 h at 37°C in 75 μl of RPMI 1640 supplemented with 2 mM glutamine, 100 U/ml penicillin, 100 μg/ml streptomycin, 50 μg/ml gentamicin, 110 μg/ml sodium pyruvate, 50 μM 2-ME, 10 mM HEPES, and 10% FCS. Splenocytes were then stimulated with IFN-α1 (BioLegend) or IL-18 (BioLegend) in a 2-fold dilution series in 75 μl of supplemented RPMI 1640, starting at 50 ng/ml or 10 ng/ml, respectively. Cells were incubated at 37°C for 15 min and then fixed using 150 μl of FluoroFix (BioLegend), followed by permeabilizing using True-Phos Perm Buffer as recommended by the manufacturer (BioLegend). Cells were then intracellularly stained with Abs against phospho-$STAT1^{Ser727}$ (S727) (clone A15158B; BioLegend) and phospho-p38 (clone 36/p48 [pT180/pY182]; BD Biosciences). Cells were then analyzed using a flow cytometer.

Determination of MCMV titer

An aliquot of MCMV at a starting concentration of 10,000 PFU/ml was diluted to 500 PFU/ml using sterile PBS and then serially diluted by 5-fold to concentration of 100 PFU/ml and 20 PFU/ml. A portion of the 20 PFU/ml aliquot was additionally diluted 2-fold to generate 10 PFU/ml. Wild-type mice were infected with 100 μl of the original 10,000 PFU/ml aliquot (i.e., 1,000 PFU), whereas Ly49H-deficient mice were infected with 100 μl of each of the four dilutions (50 PFU, 10 PFU, 2 PFU, and 1 PFU). At 7 DPI, the mice were euthanized and spleens recovered. Spleens were weighed before being mechanically dissociated through a 40-μm cell strainer and suspended in DMEM. DNA was isolated from a portion of the splenocyte suspension using the ReliaPrep Blood gDNA Miniprep Kit (Promega) according to the manufacturer's instructions. Real-time PCR was performed with the SYBR Green Master Mix reagent (Invitrogen) under standard conditions. Primers were designed to detect the IE1 gene of MCMV (forward primer: 5′-AGCCACCAACATTGACCACGCAC-3′; and reverse primer: 5′-GCCCCAACCAGGACACACAACTC-3′). Copies per reaction were determined and used to calculate the estimated number of copies of IE1 DNA per milligram of spleen (37).

Statistical analysis

Statistical analyses were made using Prism v9 (GraphPad Software). Most comparisons were evaluated by two-way ANOVA with the Benjamini and Yekutieli correction, matching cellular subsets isolated from the same mice when possible. Results with $p < 0.05$ were considered significant. Error bars represent SD from the mean unless otherwise noted.

Results

Group 1 ILCs form six major subsets

We devised a 36-marker mass cytometry panel tailored toward group 1 ILCs (panel 1), which includes NK cells and ILC1, and first examined splenocytes from uninfected 8-wk-old B6 mice. A total of 29,800 group 1 ILCs ($CD2^+CD3^-CD19^-2B4^+NK1.1^+CEACAM\text{-}1^{lo/-}$) were clustered by viSNE (35) and analyzed by FlowSOM (36) to identify different metaclusters within the data (Fig. 1A). Repeated testing showed isolation of ILC1s as a distinct subset required a minimum of 13 metaclusters. These ILC1s were $CD49b^{+/-}CD11b^-CD27^+$ and expressed higher levels of CD69, CD127, and CD200R1 (Fig. 1B), as previously reported (38–40). We additionally found ILC1s to express significantly more CD96, CD132, DNAM-1, NKp46, and NKR-P1B compared with all NK cell subsets and more IL18Ra and NKG2D than all but one NK cell subset (Supplemental Fig. 2). The remaining 12 metaclusters were all $CD49b^+CD127^{lo/-}CD200R1^-$ NK cells. However, five pairs of clusters (M2a/b, M3b/c, M4a/b, M5a/b, and M6a/b) differed according to the same dichotomy: preferential expression of activating Ly49 receptors or NKG2ACE (Fig. 1B). Similarly, cells bound or unbound by the Ab clone 5E6, an Ab capable of recognizing both Ly49C and Ly49I [though limited to Ly49I recognition in B6 mice (31)], drove two other bifurcation events (M3a/bc and M4ab/c). These repetitive events suggested an overpartitioning of NK cell subsets, albeit one necessary to draw out the ILC1 population. Omitting these distinctions simplified the 12 NK cell clusters into 5.

These five subsets could then be efficiently separated using CD90 and two other markers associated with different stages of NK cell differentiation, KLRG1 and Ly6C (29, 41). Two types of naive $KLRG1^-Ly6C^-$ NK cells were present, with the most prominent difference being high or low expression of CD90. The $CD90^{hi}$ clusters stained strongly for CD27, whereas the trio of $CD90^{lo}$ clusters had middling expression of both CD27 and CD11b (Fig. 1C). This identified the $CD90^{hi}$ subset as an immature subset and the $CD90^{lo}$ as an "intermediate" or "transitioning" subset that had not fully matured into $CD11b^+CD27^{lo/-}$ cells (42). KLRG1 is upregulated on Ag-experienced, fully mature $CD11b^{hi}CD27^{lo/-}$ NK cells (41), and

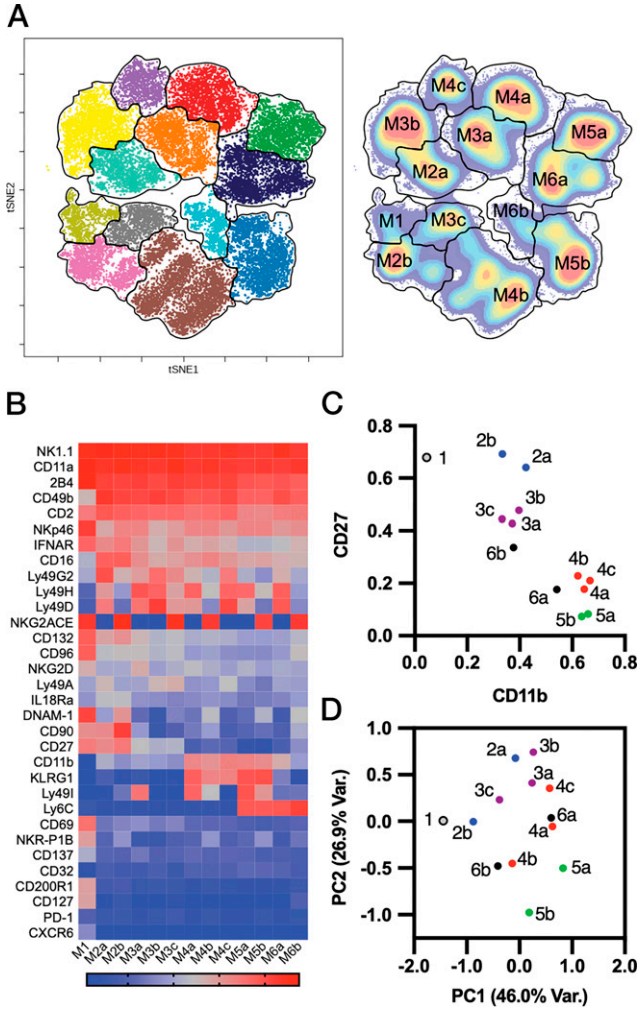

FIGURE 1. Steady-state composition of splenic group 1 ILC compartment. (**A**) viSNE map and associated density plot of splenic group 1 ILCs from uninfected B6 mice ($n = 4$), colored by metacluster. (**B**) Heat map displaying the phenotype of each of the 13 metaclusters. Metacluster values represent the weighted average of cluster medians normalized as percentage of global maximum. (**C**) Maturation status of the group 1 ILC metaclusters according to CD11b and CD27 expression. (**D**) PCA of metaclusters present in healthy wild-type B6 mice. Data presented are from a single experiment but are consistent with data generated in four total experiments.

the two KLRG1$^+$ groups identified were split according to the expression or absence of Ly6C. Notably, the KLRG1$^+$Ly6C$^+$ phenotype is closely associated with the long-lived memory NK (mNK) cell population present after MCMV infection (29). Combined, these four groups provide a putative sequence of phenotypes depicting NK cell differentiation from an immature subset to a memory state: KLRG1$^-$Ly6C$^-$CD90^{hi} → KLRG1$^-$Ly6C$^-$CD90^{lo} → KLRG1$^+$Ly6C$^-$ → KLRG1$^+$Ly6C$^+$.

The fifth NK subset had a phenotype of KLRG1$^-$Ly6C$^+$, which has not been previously characterized. Most features of the KLRG1$^-$Ly6C$^+$ subset (e.g., NKp46^{lo}, IFNAR^{lo}, CD2^{lo}) were shared with at least one other subset, but there was no consistency in which subset that was (Supplemental Fig. 2). Based on CD11b and CD27 expression, these cells split between intermediate and fully mature subsets (Fig. 1C). However, PCA paired them most closely with the fully mature KLRG1$^+$Ly6C$^-$ subset (Fig. 1D). Thus, KLRG1$^-$Ly6C$^+$ cells represent a third fully mature NK cell subset. It remains unclear where the KLRG1$^-$Ly6C$^+$ subset might reside in the NK cell differentiation pathway or if it follows an entirely alternative pathway. In summary, clustering analysis identified six major group 1 ILC subsets: ILC1s, immature CD90^{hi} KLRG1$^-$Ly6C$^-$ NK cells, transitionary CD90^{lo}KLRG1$^-$Ly6C$^-$ NK cells, Ag-experienced KLRG1$^+$Ly6C$^-$ NK cells, a pre-existing population with a memory-like KLRG1$^+$Ly6C$^+$ phenotype, and a novel KLRG1$^-$Ly6C$^+$ subset.

Most Ly49I$^+$ NK cells in uninfected mice have differentiated into less responsive states

Approximately 75% of the NK cells with a "memory-associated" KLRG1$^+$ Ly6C$^+$ phenotype in uninfected mice were 5E6-positive (hereafter Ly49I$^+$), accounting for just over one third of all Ly49I$^+$ cells (Fig. 2A). If these cells represent a pool of pre-existing memory-like NK cells established against unknown Ags, then the dominance of unlicensed NK cells during MCMV infection could, in part, be due to the diminished ability of memory and memory-like NK cells to respond to cytokines and heterologous stimuli (43, 44). Consistent with this possibility, these pre-existing KLRG1$^+$Ly6C$^+$ cells were CD132^{lo}, IFNAR^{lo}, and IL18Ra^{lo} relative to both immature NK cell subsets (Fig. 2B). We, therefore, measured phosphorylation of p38-MAPK and STAT1 (S727) following in vitro stimulation of B6 splenocytes with PMA plus ionomycin, IL-18, or IFN-α. Reduced levels of phosphorylation were evident in KLRG1$^+$Ly6C$^+$ cells relative to the other subsets after PMA plus ionomycin treatment, as well as after IL-18 and IFN-α exposure. Interestingly, stimulation with IL-18 resulted in STAT1 phosphorylation (Fig. 2C) despite STAT1 not being a known downstream effector of the IL-18R signaling pathway (45). STAT3, however, is phosphorylated via the MAPK cascade initiated by IL-18 signaling (46), so further cross-talk with STAT pathways is not farfetched. Regardless, the reduced responsiveness of the KLRG1$^+$Ly6C$^+$ subset to chemical and cytokine stimulation was consistent with characterization of the cells as a pre-existing memory-like NK (pemNK) cell population. Thus, the unlicensed NK cell response dominates during infection not just because Ly49I inhibits proliferation (17), but also because most Ly49I$^+$ cells have predifferentiated into less responsive Ag-experienced or memory-like states.

Development of pre-existing memory-like NK cells is not dependent upon the commensal microbiota

Despite being an inhibitory receptor, Ly49I's overrepresentation in the pemNK cells (Fig. 2A) suggested it may be key to the formation of this subset, and lending credence to this hypothesis is Ly49I's reported role in NK cell memory development to haptens (47). Upon investigation, Ly49I's mean signal intensity (MSI) of staining resembled that of Ly49H on MCMV-specific mNK cells in being significantly elevated on Ly49I$^+$KLRG1$^+$Ly6C$^+$ cells (Fig. 3A). No other receptor was immediately apparent as a driver of differentiation into KLRG1$^+$Ly6C$^+$ cells based on this criterion (Supplemental Fig. 3), including NKG2A, which has been reported as a licensing molecule (15). We also considered whether the Ly49I$^-$KLRG1$^+$Ly6C$^+$ population may be Ly49C$^+$ but appear to be unlicensed due to epitope masking resulting from a strong *cis*-interaction between Ly49C and the MHC-I alleles expressed in B6 mice (31, 48, 49). Upon studies comparing NK cell phenotypes with the 5E6 Ab, the Ly49C-specific 4LO3311 Ab (a generous gift from Dr. Wayne Yokoyama) and the commercially available Ly49I-specific YL1-90 Ab, we found 15–30% of licensed NK cells did go undetected by the 5E6 Ab due to epitope masking. However, ~20% of KLRG1$^+$Ly6C$^+$ cells remained absent of both Ly49C and Ly49I expression when stained with the 4LO3311 and TL1-90 Abs (Fig. 3B), closely approximating the contribution of 5E6$^-$ cells to the subset, as determined earlier (Fig. 2A). Staining using the 4LO3311

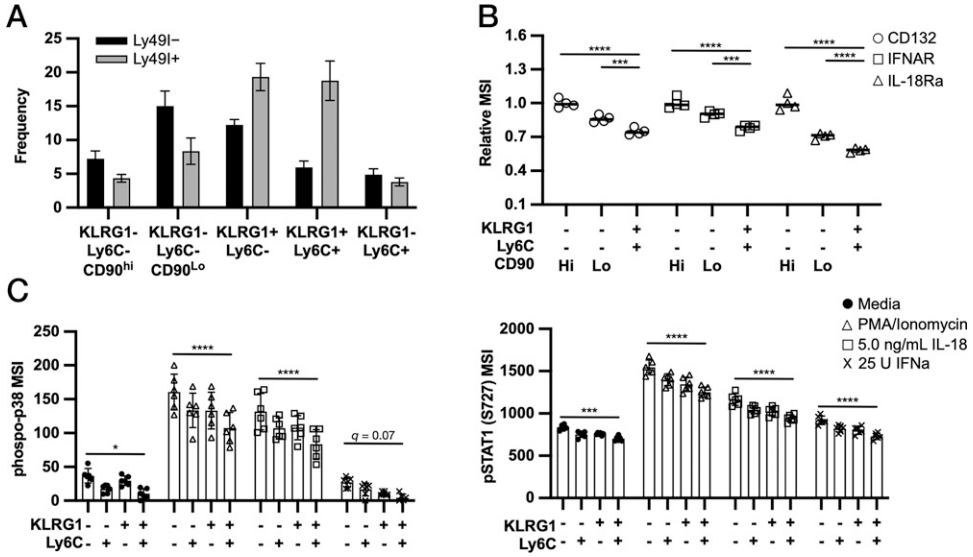

FIGURE 2. Most licensed NK cells in uninfected mice have differentiated into less responsive NK cell subsets. (**A**) Distribution of Ly49I$^+$ and Ly49I$^-$ NK cells among the five NK cell subsets as a percentage of the total NK cell population. Data shown reflect results from four mice in a single CyTOF run but are consistent with data acquired in three additional experiments. (**B**) Expression of cytokine receptors on immature KLRG1$^-$Ly6C$^-$ and fully mature KLRG1$^+$Ly6C$^+$ NK cells. Intensity reported relative to KLRG1$^-$Ly6C$^-$CD90^{hi} population. (**C**) Phosphorylation of p38 and STAT1 in NK cell subsets after treatment with PMA plus ionomycin, IL-18, or IFN-α. Signal intensity measured by flow cytometry. Data acquired in triplicate. *$p < 0.05$, ***$p < 0.001$, ****$p < 0.0001$ by repeated-measures two-way ANOVA for (B) and ordinary two-way ANOVA for (C).

and YL1-90 Abs further revealed that only Ly49I exhibited an increased expression density on KLRG1$^+$Ly6C$^+$ cells (Fig. 3C). Ly49C, like NKG2A (Supplemental Fig. 3), was expressed to a lesser extent on pemNK cells than naive NK cells (Fig. 3C).

We briefly sought the potential immunogen for Ly49I$^+$ pemNK cells in naive mice, hypothesizing that the commensal microbiota might be involved due to its effect in boosting the frequency of KLRG1$^+$NK cells (37) and a suggested relationship to "trained" innate immune memory (50). However, when we analyzed germ-free mice alongside conventionally housed B6 mice, the germ-free mice also possessed these KLRG1$^+$Ly6C$^+$ NK cells (Fig. 3D); there was actually a small, but significant, increase in their frequency compared with conventionally housed mice. Moreover, Ly49I was found on germ-free pemNK cells at the same frequency as pemNK cells from conventionally housed mice, further diminishing the likelihood that interactions with microbial byproducts produce this subset in B6 mice and suggesting microbiota does not affect licensing (Fig. 3E). The MSI of Ly49I was lower on germ-free pemNK, but it was nevertheless still elevated relative to naive NK cells (Fig. 3D). Other differences between naive and these KLRG1$^+$Ly6C$^+$ cells in CD2, IFNAR, IL18Ra, NK1.1, and other markers were all still present in germ-free mice as well (Fig. 3F). These data were therefore inconsistent with a driving role for the commensal microbiota in pemNK development.

NKR expression levels vary between licensed and unlicensed cells at steady state

Although the relative lack of KLRG1$^-$Ly6C$^-$Ly49I$^+$ NK cells provides an additional explanation for the preferential expansion of unlicensed cells during MCMV infection, we also addressed whether pre-existing differences in phenotype within subsets might contribute. For that, we examined the CD90^{lo}KLRG1$^-$Ly6C$^-$ and KLRG1$^+$Ly6C$^-$ clusters, each of which separated into two groups based on Ly49I status (Fig. 1B). Within each of these cluster pairs, Ly49A, Ly49D, Ly49G2, and NKR-P1B all appeared more frequently on Ly49I$^-$ NK cells (Fig. 4A) and at higher MSI when present (Fig. 4B). There was an important exception to this pattern among the Ly49 receptors: Ly49H. There was no preferential distribution among Ly49I-positive or -negative cells, but Ly49H was expressed at a higher density on Ly49I$^+$ cells. NKp46 and NKG2D were similar to Ly49H in that manner, also being expressed more robustly on licensed NK cells. Given the more limited expression of NKR-P1B, an inhibitory receptor engaged by the MCMV immunoevasin m12 (51), and an increased expression of the activating NKRs Ly49H, NKG2D, and NKp46, these data would argue for an *increased* potential of licensed Ly49I$^+$ NK cells to respond during MCMV infection. These data, therefore, suggest pre-existing phenotypic differences between licensed and unlicensed cells, when accounting for cellular maturity, do not explain the disparate NK cell responses to MCMV.

A subset of Ly49H$^+$ NK cells lose expression of CD16 and NK1.1 during the NK cell expansion phase

Following the characterization of licensed and unlicensed cells at steady state, we investigated changes in these cells during MCMV infection. Groups of B6 mice received 1000 PFU of salivary gland-derived MCMV, and splenocytes from 4, 7, 14, and 35 DPI were analyzed alongside uninfected controls. Immediately apparent was the significant downregulation of two key group 1 ILC lineage markers: NK1.1 and NKp46 (Fig. 5A). This necessitated a revision of the group 1 ILC phenotype to identify responding NK cells as CD2$^+$CD3$^-$CD8$^-$CD19$^-$2B4$^+$CEACAM-1$^{lo/-}$ to avoid excluding NK cells in the analysis. A resulting total of 72,785 cells (14,557 per time point) were analyzed by viSNE. Examination of the plots revealed that a few contaminating myeloid and NKT cells were present (Fig. 5B), though they combined for no more than 2.5% of the cells at any time point. Thus, the alternative gating strategy was highly effective at isolating group 1 ILCs without using the traditional NK cell lineage markers for identification of responding NK cells.

Both the Ly49I$^+$ and Ly49I$^-$ NK cells underwent considerable phenotypic change during infection before returning to a near preinfection state, with the key difference being the expected increase in mNK cells (Fig. 5C, 5D). The nonstandard gating strategy additionally revealed the presence of a small group of CD49b$^+$Ly49H$^+$ NK1.1$^-$CD16$^-$ NK cells at 4 DPI (Fig. 5E). Though more easily seen in the Ly49I$^-$ subset, these cells were present in both groups. Because NK1.1 and CD16 depend upon FcεRIγ for surface

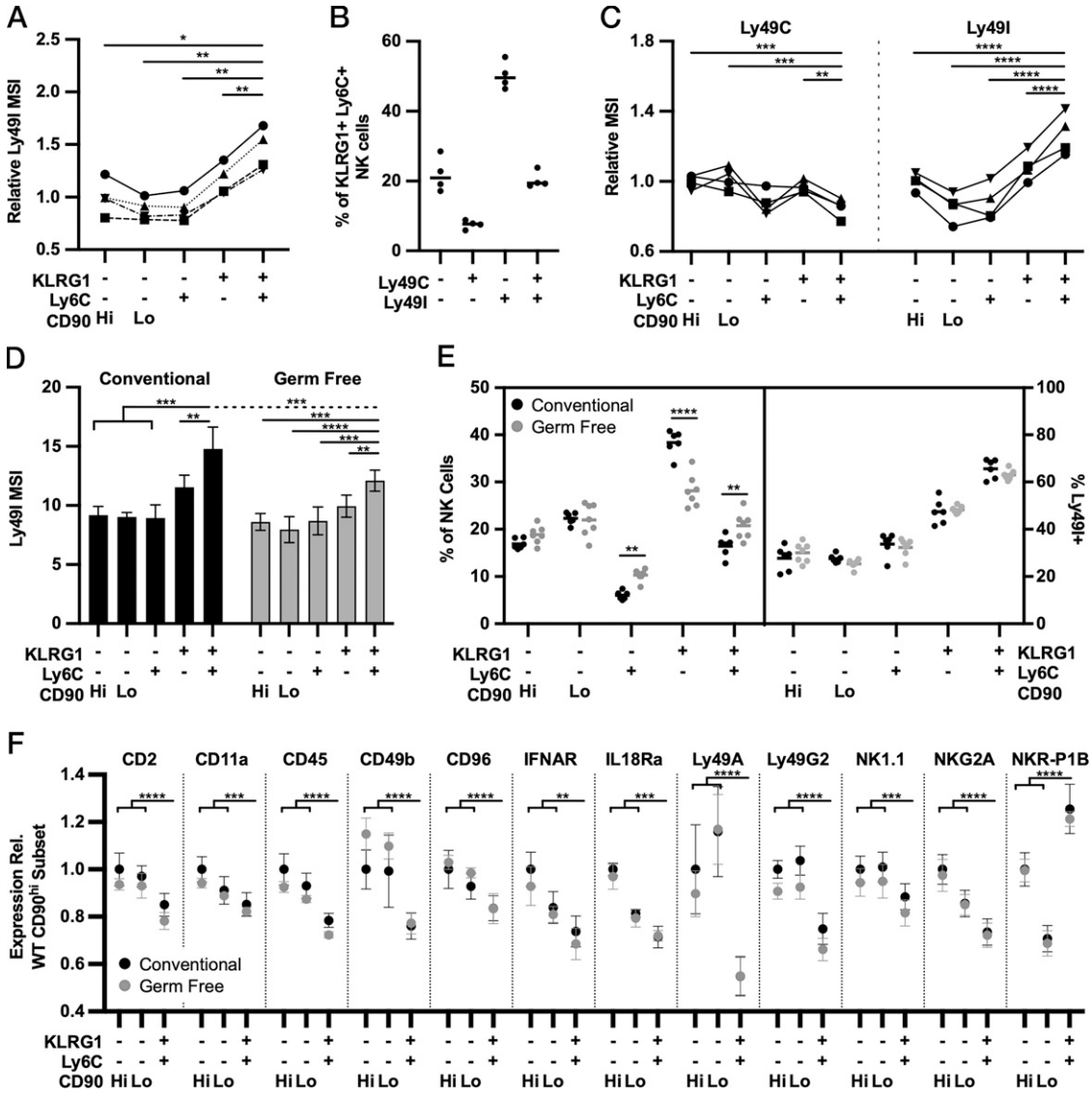

FIGURE 3. Pre-existing memory-like NK cells develop in conventionally housed and germ-free mice. (**A**) Relative MSI of Ly49I on NK cell subsets as determined by the 5E6 Ab. Data are representative of a single experiment ($n = 4$), but consistent with analysis of five additional experiments using both CyTOF and flow cytometry. (**B**) Frequency of Ly49C and Ly49I on KLRG1$^+$Ly6C$^+$ NK cells alone or in tandem using Ly49C-specific (clone 4LO331) and Ly49I-specific (YL1-90) Abs. (**C**) Relative MSI of Ly49C and Ly49I on KLRG1$^+$Ly6C$^+$ NK cells determined with the 4LO331 and YL1-90 Abs. $n = 4$ mice, experiment repeated in duplicate. (**D**) Relative MSI of Ly49I on splenic NK cells from conventionally housed ($n = 6$) and germ-free mice ($n = 7$). Data presented from a single CyTOF run. (**E**) Distribution of NK cells among the five NK cell subsets (left) and frequency of Ly49I$^+$ NK cells within each of those subsets (right). (**F**) Phenotypic differences between naive KLRG1$^-$Ly6C$^-$ NK cells and pemNK cells, shown as expression intensity relative to KLRG1$^-$Ly6C$^-$CD90^{hi} cells from conventionally housed mice. *$p < 0.05$, **$p < 0.01$, ***$p < 0.001$, ****$p < 0.0001$.

expression, and a subset of NK cells in humans is known to downregulate FcεRIγ following human CMV infection (52, 53), we examined whether these might be a corresponding population in mice. Though we confirmed that 8–10% of CD2$^+$CD3$^-$CD8$^-$CD19$^-$CEACAM-1$^-$2B4$^+$CD49b$^+$Ly49H$^+$ cells were NK1.1$^-$CD16$^-$ at 4 DPI (Fig. 5F), such lymphocytes nevertheless retained expression of FcεRIγ at levels equivalent to NK1.1$^+$CD16$^+$ cells (Fig. 5G). The loss of NK1.1 and CD16 expression on these cells was therefore not due to silencing of the FcεRIγ signaling adapter, which occurs in human NK cells responding to CMV.

Licensed and unlicensed cells phenotypically converge during MCMV infection

For the detailed comparison of changes to licensed and unlicensed NK cell phenotypes during primary MCMV infection, NK cells were divided into four populations on the basis of Ly49I and Ly49H expression. Although there were observable differences in Ly49H$^+$ and Ly49H$^-$ cells, overt cellular phenotypes showed minimal differences between licensed and unlicensed NK cells (Fig. 6A). PCA confirmed that Ly49I$^+$ and Ly49I$^-$ populations became more similar to one another at all time points postinfection compared with preinfection, regardless of Ly49H status (Fig. 6B, 6C). However, the extent and duration of that similarity did differ between Ly49H$^+$ and Ly49H$^-$ cells. Non-Ag–specific Ly49I$^+$ and Ly49I$^-$ responses peaked in similarity at 4 DPI before beginning to diverge again, whereas licensed and unlicensed Ly49H$^+$ NK cells continued to increase in resemblance through 7 DPI and remained highly similar into the memory phase (Fig. 6C). The separation that developed between licensed and unlicensed cells in the Ly49H$^-$ compartment could be at least partially attributed to a disproportionate influx of

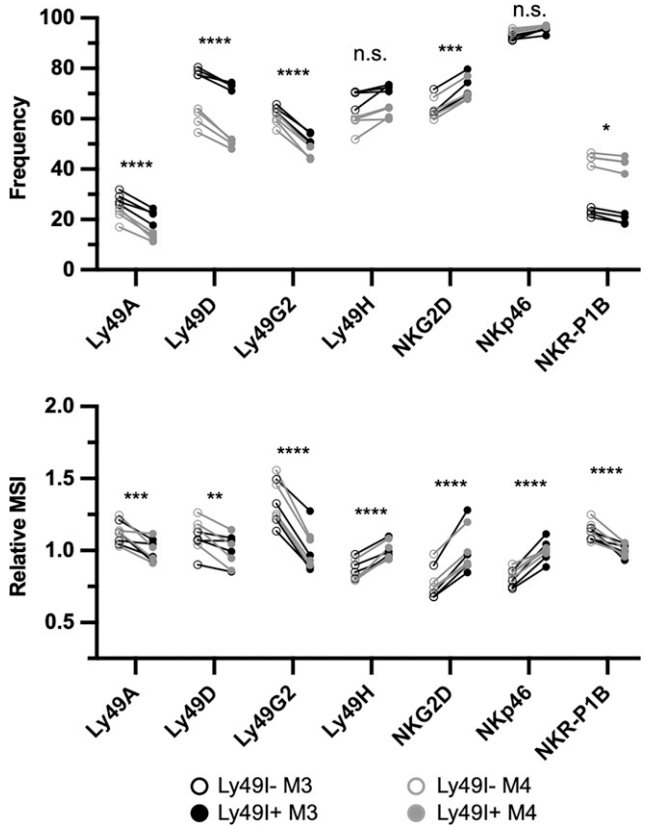

FIGURE 4. Licensed and unlicensed NK cells of similar differentiation status have different NKR expression patterns. Expression frequency (top) and MSI (bottom) of NKRs on Ly49I$^+$ and Ly49I$^-$ cells. Intensity measurements reported relative to the MSI of Ly49I$^+$KLRG1$^-$Ly6C$^-$CD90^{lo} cells. Data presented from a single experiment but are representative of three additional CyTOF runs. *$p < 0.05$, **$p < 0.01$, ***$p < 0.001$, ****$p < 0.0001$.

newly generated naive KLRG1$^-$Ly6C$^-$ cells between licensed and unlicensed cells, whereas the Ly49H$^+$ subsets maintained a similar balance (Fig. 6D).

Ultimately, there were very few differences in phenotype between Ly49I$^+$ and Ly49I$^-$ cells during the response. Some of these carried over from the steady state, such as the continued higher expression of NKp46 and NKG2D on licensed NK cells. The remaining inequalities were evident at singular time points, with nearly all occurring at 4 DPI. These differences at 4 DPI were in Ly49H, Ly49D, IL18Ra, and CD69 (Fig. 7A). Specifically, selection for higher avidity Ly49H$^+$ NK cell clones was already evident in licensed NK cells at 4 DPI, but not in unlicensed NK cells; unlicensed cells instead had a slight increase in frequency of Ly49D$^-$Ly49H$^+$ NK cells. IL-18Ra was more significantly downregulated on Ly49I$^+$ NK cells, and especially on Ly49I$^+$Ly49H$^-$ NK cells. Both Ly49H$^+$ and Ly49H$^-$Ly49I$^+$ cells displayed higher cell surface expression for the early activation marker CD69 than their Ly49I$^-$ counterparts. These observations of licensed NK cells were true only for Ly49I$^+$ NK cells and not Ly49C$^+$ NK cells. Ly49C$^+$Ly49I$^-$ cells tracked more closely in differentiation status with unlicensed cells than Ly49I$^+$ cells (Fig. 7B, 7C) and expanded to a similar magnitude as unlicensed Ly49H$^+$ NK cells during infection (Fig. 7D). Though ostensibly surprising, these results were in actuality consistent with other work that found *cis* interactions between inhibitory Ly49s and MHC-I weakens or ablates the effects of that Ly49 on NK cell function (48, 54). Lastly, one additional difference observed between Ly49I$^+$ and Ly49I$^-$ cells was in CD16 expression at the memory time point (35 DPI). A small, but significant, percentage of Ly49I$^-$ NK cells downregulated expression of CD16, whereas no significant change was seen in the Ly49I$^+$ NK cells (Fig. 7E).

The phenotypes of pemNK cells and MCMV-specific mNK cells are highly similar

The unlicensed mNK cell population expanded more than 4-fold from 2.7% of group 1 ILCs preinfection to 11.8% postinfection, whereas the licensed Ly49I$^+$ mNK population only increased by 1.25-fold (Fig. 5C). Because the CD16 phenotype at 35 DPI was predominant in unlicensed cells (Fig. 7E), we examined whether the two findings were interrelated. Indeed, the CD16$^-$ phenotype revealed itself within the unlicensed KLRG1$^+$Ly6C$^+$ mNK cell population (Fig. 8A). The Ly49I$^-$KLRG1$^-$Ly6C$^+$ population also appeared to have more CD16$^-$ cells; however, the difference was nonsignificant. The licensed CD16$^+$ mNK cells also decreased in frequency compared with uninfected mice, implying that the development of a CD16$^-$ mNK population is not prevented by licensing. However, there was clear favoritism for the unlicensed NK cells. Whether *cis*- or *trans*-interactions between inhibitory Ly49 molecules and MHC-I affect the formation of the small CD16$^-$ subset remains an outstanding question.

This unequal distribution of CD16$^-$ cells in licensed versus unlicensed mNK cells prompted further scrutinization of the memory populations for other changes. Although we confirmed that the CD16 phenotype was the major difference between the Ly49I$^+$ and Ly49I$^-$ subsets, other significant observations were recorded. Most of the phenotypes identified on pemNK in naive mice (Fig. 3F) were also present on all KLRG1$^+$Ly6C$^+$ cells after MCMV infection, occasionally becoming slightly more exaggerated, such as in CD49b, CD132, IFNAR, and IL18Ra (Fig. 8B). The Ly49H$^-$ NK cells postinfection fully recapitulated the pemNK phenotypes observed in naive mice. Postinfection Ly49H$^+$ mNK cells, however, no longer expressed less CD96 and NK1.1 compared with naive cells and also developed three new memory cell–associated phenotypes. These were an increased MSI of Ly49H, a loss of DNAM-1, and a decrease in NKR-P1B frequency, all of which are consistent with previous characterizations of MCMV-specific NK cell memory (29, 51, 55).

Licensed and unlicensed responses to MCMV converge regardless of specific recognition of MCMV-infected cells

In mice lacking the Ly49H receptor, the absence of an Ag-specific NK cell response during primary MCMV infection is known to affect inflammatory cytokine production and splenic dendritic cell abundances (56), both of which can critically impact NK cell maturation and function (57–59). Moreover, that the Ly49H$^+$Ly49I$^+$ mNK cells resembled the Ly49H$^+$Ly49I$^-$ population, more so than the Ly49H$^-$Ly49I$^+$ subset (Fig. 8B), suggested that signaling through Ly49H might obscure any differences in licensed and unlicensed NK cells responses to a viral infection. We therefore investigated responses in mice lacking the Ly49H receptor. *Klra8*$^{-/-}$ (Ly49H-deficient) B6 mice were infected alongside wild-type B6 mice and analyzed with an updated mass cytometry panel (panel 2). Because mice lacking Ly49H are more susceptible to MCMV, the Ly49H-deficient B6 mice received 1/1000th the dose given to wild-type B6. This yielded a similar, though still ~2-fold higher, viral load in Ly49H-deficient mice at 7 DPI (Supplemental Fig. 4) and prevented excessive splenic tissue destruction. Observations of responses in wild-type B6 mice made previously were confirmed with the updated panel, including superior resolution of the NK1.1$^{lo/-}$CD16$^-$ population at 4 DPI (Fig. 9A, 9B, metaclusters B and C). The new panel also included the checkpoint receptors TIGIT and LAG-3,

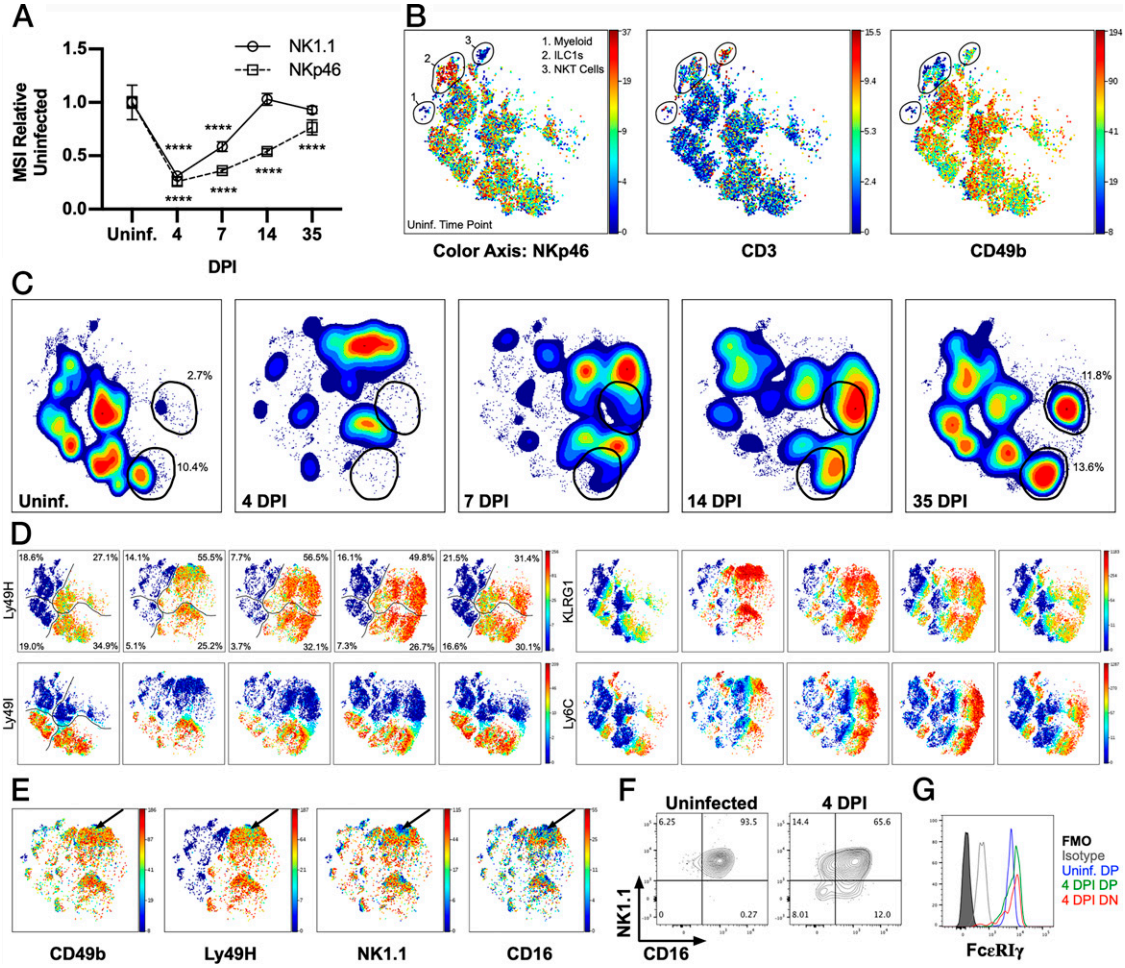

FIGURE 5. An alternative gating strategy for group 1 ILCs reveals an NK1.1$^-$CD16$^-$ NK cell population at 4 DPI. (**A**) NK1.1 and NKp46 expression intensities relative to uninfected mice. Data shown from a single experiment but representative of four total. ****$p < 0.001$. (**B**) Example plot demonstrating the fidelity of a gating strategy for group 1 ILCs that does not make use of NK1.1 or NKp46. Plots are colored according to NKp46 (left), CD3 (middle), and CD49b (right). (**C**) Density plots showing the dynamic changes in group 1 ILCs during MCMV infection. Gated areas demarcate KLRG1$^+$Ly6C$^+$ memory and memory-like populations. (**D**) Ly49H, Ly49I, KLRG1, and Ly6C expression on group 1 ILCs during MCMV infection. Percentages in the Ly49H plots correspond to the Ly49H$^-$Ly49I$^-$ (top left), Ly49H$^-$Ly49I$^+$ (bottom left), Ly49H$^+$Ly49I$^-$ (top right), and Ly49H$^+$Ly49I$^+$ population frequencies at the respective time points. (**E**) Evidence of a CD49b$^+$Ly49H$^+$NK1.1$^-$CD16$^-$ NK cell population (arrows) at 4 DPI. (**F**) Identification of NK1.1$^-$CD16$^-$ by flow cytometry and (**G**) subsequent confirmation of FcεRIγ expression. Data shown from a representative animal from a pool of four mice. DN, NK1.1$^-$CD16$^-$ subset; DP, NK1.1$^+$CD16$^+$ subset; FMO, fluorescence-minus-one control.

which, like PD-1 (Fig. 6A), were not found on any mNK populations (metaclusters M and N).

Although the Ly49H-deficient mice exhibited a clearly distinct response from wild-type mice (Fig. 9A, 9B), licensed and unlicensed cells within the non–Ag-specific NK cell response still converged just as in wild-type mice (Fig. 9C). The pattern of their relationship closely mirrored that of Ly49H$^-$ NK cells in wild-type mice, with the notable exception of Ly49I$^+$ and Ly49I$^-$ cells in Ly49H-deficient mice becoming more dissimilar at 28 DPI than they were in uninfected mice. We attribute this to the much higher frequency of KLRG1$^-$Ly6C$^-$ NK cells in Ly49H-deficient mice and a corresponding reduced frequency of Ly49I$^+$ and KLRG1$^+$ Ly6C$^+$ cells (Fig. 9D). This distribution weighted toward undifferentiated NK cells likely reflected a more limited history of pathogen exposure, similar to how NK cell diversity in humans varies according to their histories of viral infections (60).

Consistent with the NK cells from wild-type mice, only select few differences between licensed and unlicensed cells were observed in Ly49H-deficient mice. Altered phenotypes in IL18Ra, CD69, and Ly49D at 4 DPI appeared in the Ly49H-deficient mice just as they did in wild-type mice, though Ly49I$^+$ cells from Ly49H-deficient mice now also saw an uptick in the frequency of Ly49D$^+$ NK cells in addition to the downregulation in the frequency of Ly49D$^+$ NK cells within the Ly49I$^-$ subset (Fig. 9E). In contrast to the wild-type cells though, a CD16$^-$ memory population did not appear in Ly49H-deficient mice (Fig. 9F). Considering the CD16$^-$ cells were concentrated in the unlicensed mNK Ly49H$^+$ population in wild-type mice and that population did not significantly expand in Ly49H-deficient mice (Fig. 9A, metacluster N), this was not altogether surprising. In summary, regardless of whether an Ag-specific NK cell response to MCMV was generated, the licensed and unlicensed NK cell responses converged upon a singular phenotype. The dominance of the unlicensed response, therefore, does not appear to be the result of any functional deficiencies we could observe by phenotyping, but rather because of the combined effects of inhibitory signaling on proliferation and a smaller pool of KLRG1$^-$Ly6C$^-$Ly49I$^+$ NK cells at the time of infection.

Discussion

In B6 mice, the NK cell compartment can be separated into licensed cells, which are Ly49C$^+$ and/or Ly49I$^+$, and unlicensed cells, which

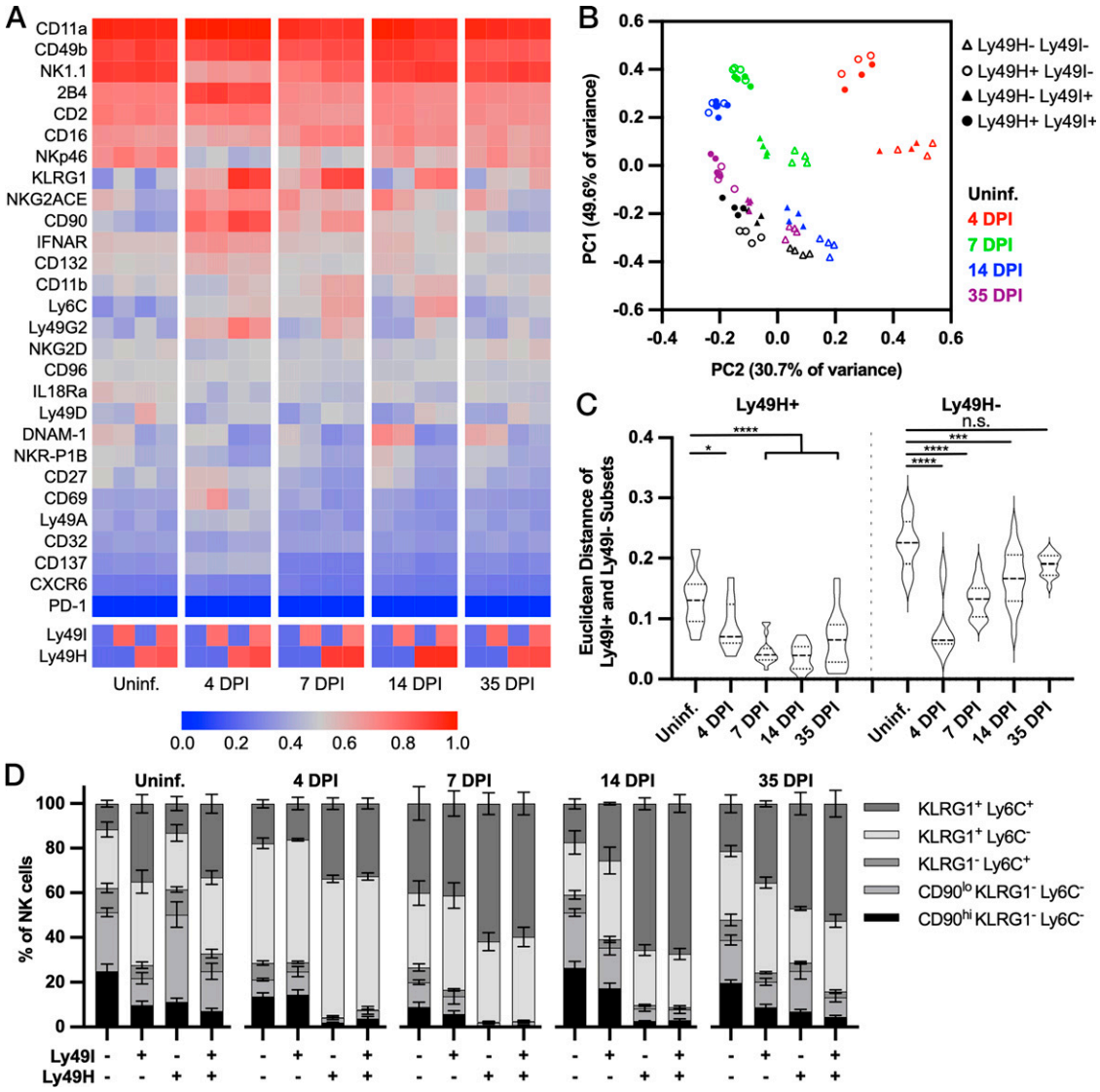

FIGURE 6. Licensed and unlicensed cells increase in similarity during MCMV infection. (**A**) Heat map of NK cell phenotypes for the four Ly49I/Ly49H populations at each time point. Individual events were normalized as percentage of global maximum, using the median of the top 100 events as the maximum value to account for outliers. (**B**) PCA of the Ly49I and Ly49H populations. (**C**) Euclidean distance between the $Ly49I^+$ and $Ly49I^-$ populations within the $Ly49H^+$ (left) and $Ly49H^-$ (right) subsets. Distance measurements were made between all possible pairings for each time point. (**D**) Distribution of NK cell subsets within each of the four Ly49I and Ly49H compartments during MCMV infection. $*p < 0.05$, $***p < 0.001$, $****p < 0.0001$.

lack both of those receptors (14, 26). Under noninflammatory conditions, licensed cells show superior functional activity in vitro, especially when presented with MHC-I–deficient target cells (15, 61, 62). Following exposure to inflammatory cytokines, however, unlicensed cells become equally functional to and, in at least some cases, better effectors than their licensed equivalents (14, 15, 17). One such example is in MCMV infection of B6 mice (17). SHP-1 recruitment following inhibitory Ly49 ligand recognition limits proliferation via Vav1 dephosphorylation (18) and, consequently, the ability of licensed NK cells to provide an optimal immune response to the virus (17). Given Vav1 has a much more extensive role in NK cell activation than just fostering proliferation (23–25), we developed and implemented a mass cytometry panel to further investigate whether licensed and unlicensed NK cell responses to MCMV were qualitatively different beyond their proliferation efficiencies.

At steady state, splenic NK cells separated into five major subsets according to their expression of the differentiation markers KLRG1 and Ly6C, with the additional separation of $KLRG1^-Ly6C^-$ cells into $CD90^{hi}$ and $CD90^{lo/-}$ subsets. Despite approximately half of all cells expressing Ly49C and/or Ly49I, the licensed and unlicensed cells were not evenly distributed among the five KLRG1/Ly6C/CD90 subsets. Unlicensed cells were much more frequently $KLRG1^-$ than $KLRG1^+$, whereas licensed cells were the opposite. Ag-experienced $KLRG1^+$ NK cells are known to be less proliferative than naive cells, regardless of licensing status (37, 41). Moreover, a significant proportion of $Ly49I^+$ cells in naive mice had the $KLRG1^+Ly6C^+$ phenotype closely resembling MCMV-specific mNK cells, and mNK cells are refractory to heterologous stimuli (43, 44). These pre-existing $KLRG1^+Ly6C^+$ NK cells in naive mice closely resembled bona fide MCMV-specific mNK cells in phenotype, having downregulated cytokine (e.g., CD132, IFNAR, IL18Ra) and costimulatory (e.g., CD2, CD11a) receptors, and similarly showed less responsiveness to cytokine stimulation in vitro. We, therefore, conclude that unlicensed NK cells dominate the response not only because their ability to proliferate is unrestricted by an inhibitory Ly49, but also because many licensed NK cells in naive mice have already differentiated into $KLRG1^+Ly6C^-$ and $KLRG1^+Ly6C^+$ NK cells that have an inherent reduced ability to proliferate and respond to unrelated immunological stimuli.

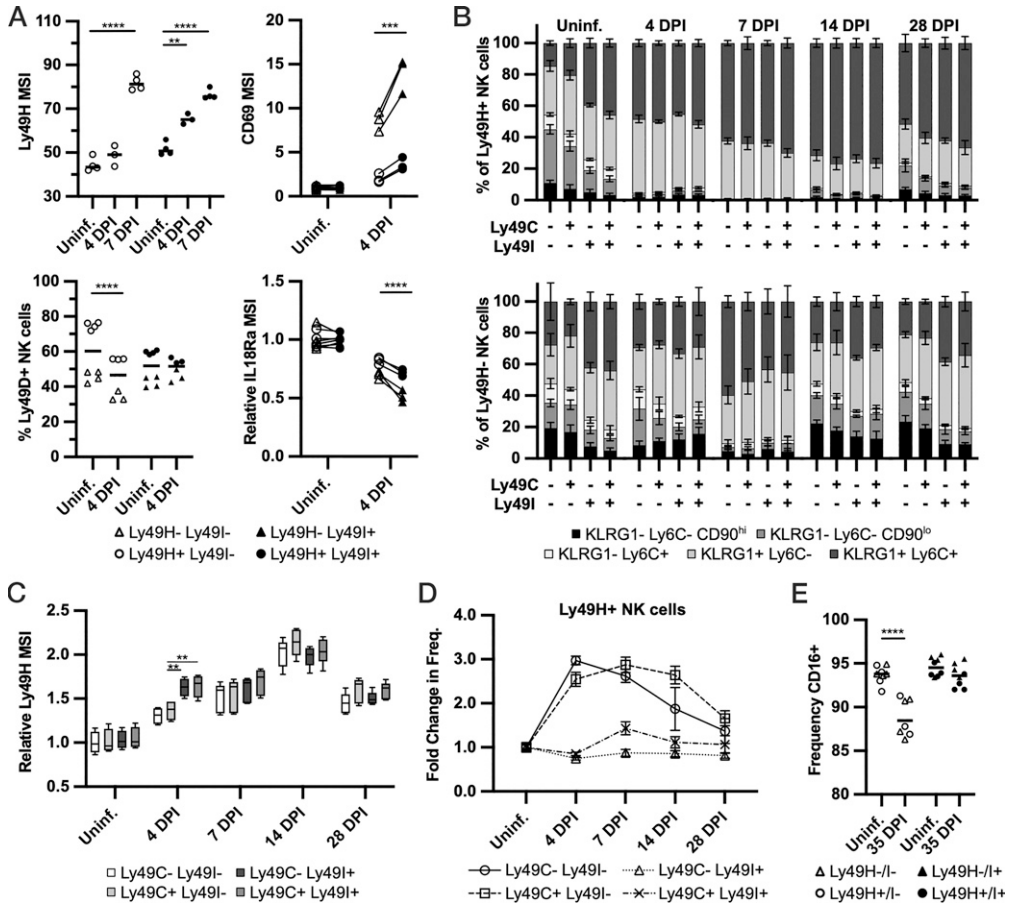

FIGURE 7. The limited variability in licensed and unlicensed NK cell responses was driven by Ly49I and not Ly49C. (**A**) Significantly different phenotypes between licensed and unlicensed NK cells at 4 DPI as separated by the 5E6 Ab. Presented experiment is one of four repetitions. (**B**) Frequency of the NK cell subsets in Ly49H$^+$ (top) and Ly49H$^-$ (bottom) NK cells separated according to the expression or absence of Ly49C and Ly49I ($n = 5$ mice). (**C**) Change to Ly49H MSI on NK cells expressing one, both, or neither of the B6 licensing receptors during MCMV infection. (**D**) Magnitude of Ly49H$^+$ NK cell expansion when coexpressing one, both, or neither of Ly49C and Ly49I. Measured as frequency of the total NK cell population at the indicated time point/frequency of total NK cell population in naive uninfected mice. (**E**) Significantly different phenotypes between Ly49I$^+$ and Ly49I$^-$ NK cells at 35 DPI. $^{**}p < 0.01$, $^{***}p < 0.001$, $^{****}p < 0.0001$.

The dissimilarities between Ly49I$^+$ and Ly49I$^-$ NK cell phenotypes, after accounting for differentiation status, further argued against licensed cells being at a disadvantage beyond the restrictions inhibitory Ly49 signaling places on proliferation. KLRG1$^-$ Ly6C$^-$Ly49I$^+$ NK cells in naive mice actually had a phenotype predictive of a *more* potent response. They expressed more of the activating receptors Ly49H, NKG2D, and NKp46 and less of the inhibitory NKR-P1B than their Ly49I$^-$ equivalents. Moreover, Ly49I$^+$ cells had a more activated phenotype at 4 DPI; selection for Ly49H^{hi} NK cell clones was already occurring, surface density of

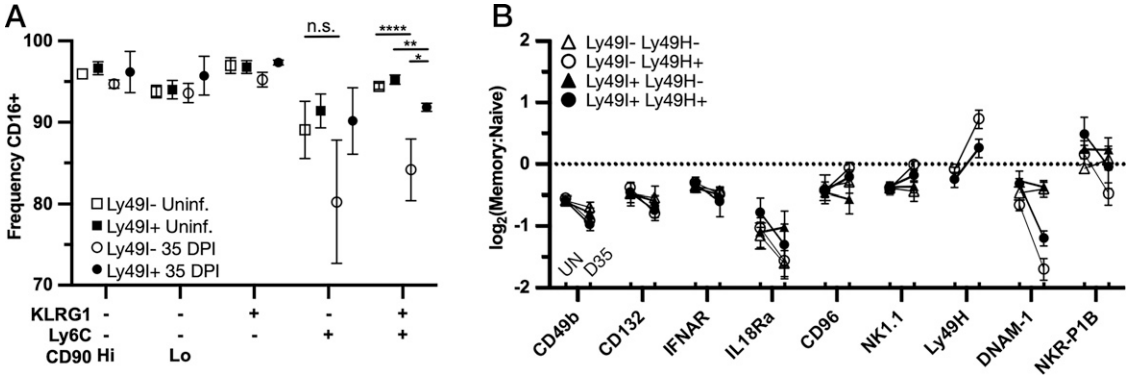

FIGURE 8. Differences in memory and memory-like populations postinfection. (**A**) Frequency of CD16$^+$ expression among licensed and unlicensed NK cell subsets in uninfected and 35 DPI mice. (**B**) Log_2-fold difference between memory/memory-like (KLRG1$^+$Ly6C$^+$) NK cells and immature (CD90^{hi}KLRG1$^-$Ly6C$^-$) NK cells for each of the four Ly49I and Ly49H subsets. Paired data points link corresponding populations in uninfected and 35 DPI mice. The dotted line at zero on the *y*-axis denotes no difference in expression between KLRG1$^+$Ly6C$^+$ and CD90^{hi}KLRG1$^-$Ly6C$^-$ populations. Data shown are the average of four mice at each time point. $^{*}p < 0.05$, $^{**}p < 0.01$, $^{****}p < 0.0001$.

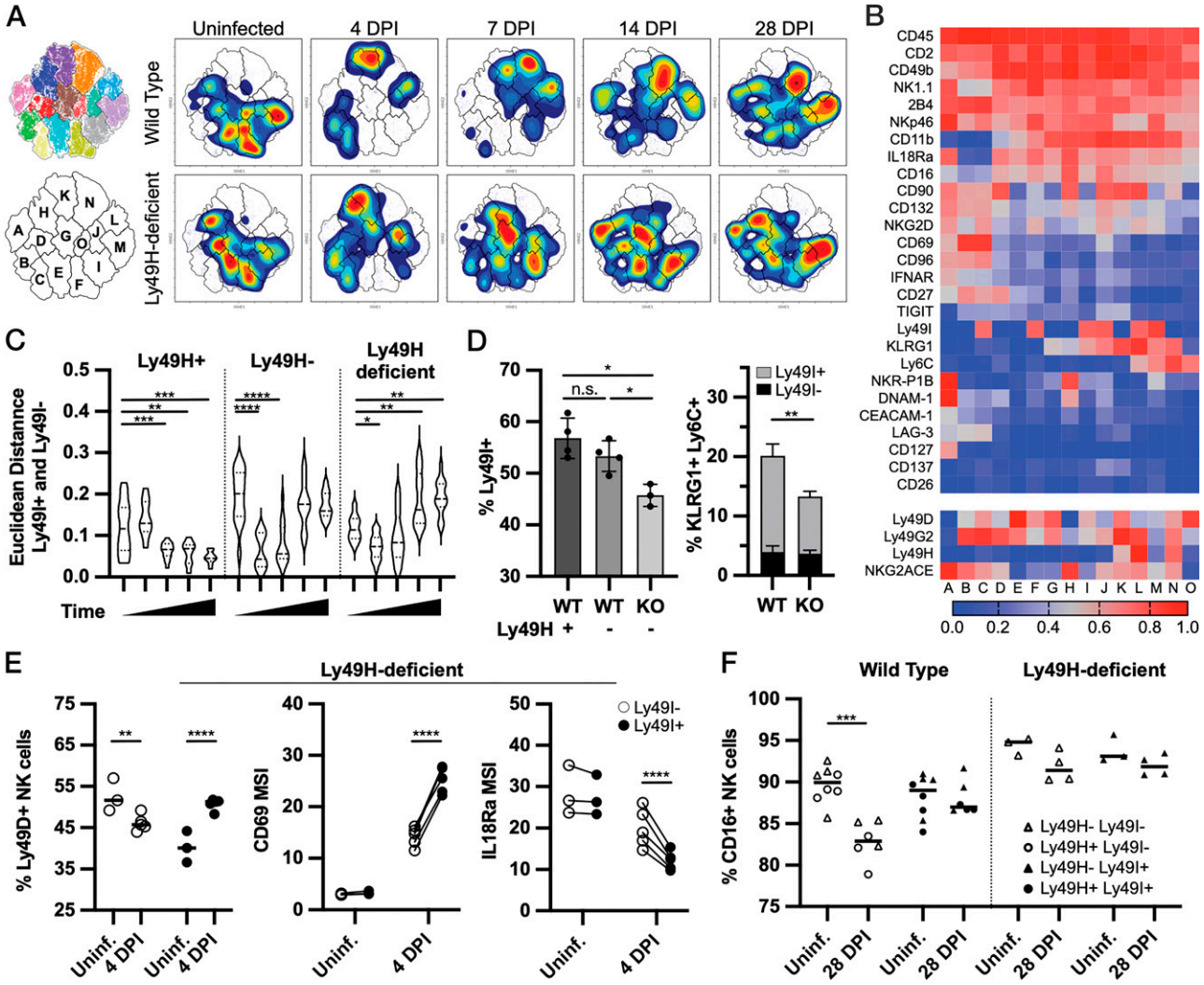

FIGURE 9. Licensed and unlicensed responses resemble one another in the absence of an MCMV-specific NK cell response. (**A**) Clustering analysis of wild-type and Ly49H-deficient group 1 ILCs. Top left shows the overlay of cells from all time points and is colored according to metacluster; the bottom left is a guide for identification of each metacluster. The remaining plots are density plots corresponding to the indicated genotype and time point. (**B**) Heat map depicting the phenotype of each metaclusters. Values represent the weighted average of constituent cluster medians normalized as percent of global maximum. (**C**) Euclidean similarity between the Ly49I$^+$ and Ly49I$^-$ populations of Ly49H$^+$ NK cells (left), Ly49H$^-$ NK cells from wild-type mice (middle), and NK cells from Ly49H-deficient mice (right). Distance measurements were made between all possible pairings for each time point. (**D**) Frequency of Ly49I$^+$ cells among the Ly49H$^+$, Ly49H$^-$, and Ly49H-deficient NK cells (left) and the breakdown of Ly49I expression in the memory-like KLRG1$^+$Ly6C$^+$ NK cells as a fraction of the total NK cell compartment in wild-type (WT) and Ly49H-deficient mice. (**E**) Phenotypic differences between licensed and unlicensed cells at 4 DPI in Ly49H-deficient mice. (**F**) Frequency of CD16$^+$ NK cells in the total licensed and unlicensed NK cell populations pre- and postinfection. All time points represent data from four mice for each genotype, except for the uninfected Ly49H-deficient samples, which had three total mice. Data shown from a single CyTOF run but are consistent with data acquired in a second experiment. $*p < 0.05$, $**p < 0.01$ $***p < 0.001$ $****p < 0.0001$.

CD69 was higher, and IL18Ra downregulation was more substantial. A model of hematopoietic stem cell transplantation and MCMV infection similarly found the kinetics of the licensed NK cell response outpaces that of the unlicensed response (63). Interestingly, in the absence of Ly49H, licensed cells exhibited an increase in Ly49D expression, another activating NKR that nonetheless lacks a ligand in this model. Combined with the observed higher expression of Ly49H on licensed cells in naive mice, these data suggest licensed NK cells might upregulate the signaling adaptor DAP12, the primary partner for Ly49H and Ly49D surface expression (64) or alternatively select for NK cell clones already expressing higher amounts of Ly49H. The functional potency of licensed NK cells is proportional to the amount of inhibitory receptor expressed (61, 62), so selection for cells with higher DAP12 expression instead of lower Ly49I expression would ostensibly yield NK cells better capable of cytokine production and target cell killing. Unlicensed cells, in contrast, need only select for clones in which there is less Ly49D, because there is no check on DAP12 signaling from inhibitory Ly49, but because Ly49D may act as a competitive inhibitor of Ly49H for DAP12. Regardless, the overall similarities in phenotype suggested that there was no apparent difference in licensed and unlicensed NK cell responses beyond the previously observed effect on proliferation magnitude (17). Moreover, we show in this study that observation is applicable only to licensing receptors that do not interact with their ligands in *cis*, a result consistent with other studies that have found *cis*-interactions stymie the inhibitory effect of Ly49A (54) and Ly49C (48). We also note that the minimal differences in licensed and unlicensed NK cell responses occurred in a model in which activating and inhibitory NKRs were not competing with one another for a ligand. The impact of licensing NKRs in such a scenario may be even less pronounced. This could be investigated in MA/My mice, in which the activating receptor Ly49P

confers resistance to MCMV via an interaction with H2-K^d (65), an MHC-I allele recognized by the inhibitory Ly49G and Ly49O receptors present in MA/My mice (66).

Ly49I also failed to impact the generation of MCMV-specific mNK cells. $Ly49H^+Ly49I^+$ and $Ly49H^+$ $Ly49I^-$ mNK were indistinguishable, except for a small pool of $CD16^-$ cells occurring preferentially in the unlicensed group. The $Ly49H^-$ memory-like NK cells postinfection recovered the same phenotype present on pemNK cells, and these $Ly49H^-$ memory-like populations had significant differences in only CD96, NK1.1, and DNAM-1 expression when compared with the MCMV-specific mNK cells. That the $Ly49I^+$ $Ly49H^+$ cells took on the phenotype of the unlicensed $Ly49H^+$ NK cells rather than the licensed $Ly49H^-$ NK cells further argued that the influence of Ly49H on NK cell memory differentiation superseded any effect signaling via inhibitory Ly49s might have caused on the memory response.

Regarding the $CD16^-$ population in the mNK cell subset at 35 DPI, it was curiously the second $CD16^-$ population to develop during the infection. The first appeared at 4 DPI, though the likelihood that this first population and the one found postinfection are related is low. Not only did the population at 4 DPI disappear before the peak of the NK cell response, but other observations also distinguished them. Specifically, the 4 DPI population was $NK1.1^{lo/-}$, whereas the mNK cells retained full NK1.1 expression. Additionally, the subset at 4 DPI appeared in both wild-type and Ly49H-deficient mice, but the $CD16^-$ memory-like NK cell population did not develop in Ly49H-deficient mice. Lastly, the $CD16^-$ population at 4 DPI was near evenly split between $Ly49I^+$ and $Ly49I^-$, whereas the mNK population was decisively more abundant in the unlicensed population. Considering stimulation of NK cells from B6 mice via CD16 is weak (67), it is unclear why such a population would develop or what advantages it might offer in the event of MCMV reactivation or reinfection.

In conclusion, based on the in-depth analysis of NK cells throughout the expansion, contraction, and memory phases of the response to MCMV in B6 mice, licensed NK cells are disadvantaged compared to unlicensed NK cells in two properties: restricted proliferation due to inhibitory Ly49 signaling resulting from ligand recognition *in trans* and a smaller abundance of readily responsive $KLRG1^-Ly6C^-$ NK cells. Future investigations should examine whether these differences extend to other viral infections and/or oncogenic events, as well as the extent to which pathogen exposure history impacts the NK cell response to novel immune challenges.

Disclosures

The authors have no financial conflicts of interest.

References

1. Sun, J. C., and L. L. Lanier. 2011. NK cell development, homeostasis and function: parallels with $CD8^+$ T cells. *Nat. Rev. Immunol.* 11: 645–657.
2. Lanier, L. L. 2008. Up on the tightrope: natural killer cell activation and inhibition. *Nat. Immunol.* 9: 495–502.
3. Raulet, D. H. 2006. Missing self recognition and self tolerance of natural killer (NK) cells. *Semin. Immunol.* 18: 145–150.
4. Held, W., and B. Kunz. 1998. An allele-specific, stochastic gene expression process controls the expression of multiple Ly49 family genes and generates a diverse, MHC-specific NK cell receptor repertoire. *Eur. J. Immunol.* 28: 2407–2416.
5. Smith, H. R. C., H. H. Chuang, L. L. Wang, M. Salcedo, J. W. Heusel, and W. M. Yokoyama. 2000. Nonstochastic coexpression of activation receptors on murine natural killer cells. *J. Exp. Med.* 191: 1341–1354.
6. Millan, A. J., B. A. Hom, J. B. Libang, S. Sindi, and J. O. Manilay. 2021. Evidence for prescribed NK cell Ly-49 developmental pathways in mice. *J. Immunol.* 206: 1215–1227.
7. Carlyle, J. R., A. Mesci, J. H. Fine, P. Chen, S. Bélanger, L.-H. Tai, and A. P. Makrigiannis. 2008. Evolution of the Ly49 and Nkrp1 recognition systems. *Semin. Immunol.* 20: 321–330.
8. Held, W., and D. H. Raulet. 1997. Expression of the Ly49A gene in murine natural killer cell clones is predominantly but not exclusively mono-allelic. *Eur. J. Immunol.* 27: 2876–2884.
9. Rouhi, A., L. Gagnier, F. Takei, and D. L. Mager. 2006. Evidence for epigenetic maintenance of Ly49a monoallelic gene expression. *J. Immunol.* 176: 2991–2999.
10. Rouhi, A., C. B. Lai, T. P. Cheng, F. Takei, W. M. Yokoyama, and D. L. Mager. 2009. Evidence for high bi-allelic expression of activating Ly49 receptors. *Nucleic Acids Res.* 37: 5331–5342.
11. Sun, J. C., and L. L. Lanier. 2008. Tolerance of NK cells encountering their viral ligand during development. *J. Exp. Med.* 205: 1819–1828.
12. Lopez-Vergès, S., J. M. Milush, B. S. Schwartz, M. J. Pando, J. Jarjoura, V. A. York, J. P. Houchins, S. Miller, S.-M. Kang, P. J. Norris, et al. 2011. Expansion of a unique $CD57^+$NKG2Chi natural killer cell subset during acute human cytomegalovirus infection. *Proc. Natl. Acad. Sci. USA* 108: 14725–14732.
13. Horowitz, A., D. M. Strauss-Albee, M. Leipold, J. +Kubo, N. Nemat-Gorgani, O. C. Dogan, C. L. Dekker, S. Mackey, H. Maecker, G. E. Swan, et al. 2013. Genetic and environmental determinants of human NK cell diversity revealed by mass cytometry. *Sci. Transl. Med.* 5: 208ra145.
14. Kim, S., J. Poursine-Laurent, S. M. Truscott, L. Lybarger, Y.-J. Song, L. Yang, A. R. French, J. B. Sunwoo, S. Lemieux, T. H. Hansen, and W. M. Yokoyama. 2005. Licensing of natural killer cells by host major histocompatibility complex class I molecules. *Nature* 436: 709–713.
15. Fernandez, N. C., E. Treiner, R. E. Vance, A. M. Jamieson, S. Lemieux, and D. H. Raulet. 2005. A subset of natural killer cells achieves self-tolerance without expressing inhibitory receptors specific for self-MHC molecules. *Blood* 105: 4416–4423.
16. Orr, M. T., and L. L. Lanier. 2010. Natural killer cell education and tolerance. *Cell* 142: 847–856.
17. Orr, M. T., W. J. Murphy, and L. L. Lanier. 2010. 'Unlicensed' natural killer cells dominate the response to cytomegalovirus infection. *Nat. Immunol.* 11: 321–327.
18. Stebbins, C. C., C. Watzl, D. D. Billadeau, P. J. Leibson, D. N. Burshtyn, and E. O. Long. 2003. Vav1 dephosphorylation by the tyrosine phosphatase SHP-1 as a mechanism for inhibition of cellular cytotoxicity. *Mol. Cell. Biol.* 23: 6291–6299.
19. Mahmoud, A. B., M. M. Tu, A. Wight, H. S. Zein, M. M. A. Rahim, S.-H. Lee, H. S. Sekhon, E. G. Brown, and A. P. Makrigiannis. 2016. Influenza virus targets class I MHC-educated NK Cells for immunoevasion. [Published erratum appears in 2016 *PLoS Pathog.* 12: e1006021.] *PLoS Pathog.* 12: e1005446.
20. Binstadt, B. A., K. M. Brumbaugh, C. J. Dick, A. M. Scharenberg, B. L. Williams, M. Colonna, L. L. Lanier, J.-P. Kinet, R. T. Abraham, and P. J. Leibson. 1996. Sequential involvement of Lck and SHP-1 with MHC-recognizing receptors on NK cells inhibits FcR-initiated tyrosine kinase activation. *Immunity* 5: 629–638.
21. Nakamura, M. C., E. C. Niemi, M. J. Fisher, L. D. Shultz, W. E. Seaman, and J. C. Ryan. 1997. Mouse Ly-49A interrupts early signaling events in natural killer cell cytotoxicity and functionally associates with the SHP-1 tyrosine phosphatase. *J. Exp. Med.* 185: 673–684.
22. Tarakhovsky, A., M. Turner, S. Schaal, P. J. Mee, L. P. Duddy, K. Rajewsky, and V. L. J. Tybulewicz. 1995. Defective antigen receptor-mediated proliferation of B and T cells in the absence of Vav. *Nature* 374: 467–470.
23. Billadeau, D. D., K. M. Brumbaugh, C. J. Dick, R. A. Schoon, X. R. Bustelo, and P. J. Leibson. 1998. The Vav-Rac1 pathway in cytotoxic lymphocytes regulates the generation of cell-mediated killing. *J. Exp. Med.* 188: 549–559.
24. Chan, G., T. Hanke, and K. D. Fischer. 2001. Vav-1 regulates NK T cell development and NK cell cytotoxicity. *Eur. J. Immunol.* 31: 2403–2410.
25. Colucci, F., E. Rosmaraki, S. Bregenholt, S. I. Samson, V. Di Bartolo, M. Turner, L. Vanes, V. Tybulewicz, and J. P. Di Santo. 2001. Functional dichotomy in natural killer cell signaling: Vav1-dependent and -independent mechanisms. *J. Exp. Med.* 193: 1413–1424.
26. Hanke, T., H. Takizawa, C. W. McMahon, D. H. Busch, E. G. Pamer, J. D. Miller, J. D. Altman, Y. Liu, D. Cado, F. A. Lemonnier, et al. 1999. Direct assessment of MHC class I binding by seven Ly49 inhibitory NK cell receptors. *Immunity* 11: 67–77.
27. Arase, H., E. S. Mocarski, A. E. Campbell, A. B. Hill, and L. L. Lanier. 2002. Direct recognition of cytomegalovirus by activating and inhibitory NK cell receptors. *Science* 296: 1323–1326.
28. Smith, H. R. C., J. W. Heusel, I. K. Mehta, S. Kim, B. G. Dorner, O. V. Naidenko, K. Iizuka, H. Furukawa, D. L. Beckman, J. T. Pingel, et al. 2002. Recognition of a virus-encoded ligand by a natural killer cell activation receptor. *Proc. Natl. Acad. Sci. USA* 99: 8826–8831.
29. Sun, J. C., J. N. Beilke, and L. L. Lanier. 2009. Adaptive immune features of natural killer cells. [Published erratum appears in 2009 *Nature* 457: 1168.] *Nature* 457: 557–561.
30. Iizuka, K., O. V. Naidenko, B. F. M. Plougastel, D. H. Fremont, and W. M. Yokoyama. 2003. Genetically linked C-type lectin-related ligands for the NKRP1 family of natural killer cell receptors. *Nat. Immunol.* 4: 801–807.
31. MacFarlane IV, A. W., T. Yamazaki, M. Fang, L. J. Sigal, T. Kurosaki, and K. S. Campbell. 2008. Enhanced NK-cell development and function in BCAP-deficient mice. *Blood* 112: 131–140.
32. Zunder, E. R., R. Finck, G. K. Behbehani, A. D. Amir, S. Krishnaswamy, V. D. Gonzalez, C. G. Lorang, Z. Bjornson, M. H. Spitzer, B. Bodenmiller, et al. 2015. Palladium-based mass tag cell barcoding with a doublet-filtering scheme and single-cell deconvolution algorithm. *Nat. Protoc.* 10: 316–333.
33. Finck, R., E. F. Simonds, A. Jager, S. Krishnaswamy, K. Sachs, W. Fantl, D. Pe'er, G. P. Nolan, and S. C. Bendall. 2013. Normalization of mass cytometry data with bead standards. *Cytometry A* 83: 483–494.

34. Kotecha, N., P. O. Krutzik, and J. M. Irish. 2010. Web-based analysis and publication of flow cytometry experiments. *Curr. Protoc. Cytom.* Chapter 10: Unit 10.17.
35. Amir, A. D., K. L. Davis, M. D. Tadmor, E. F. Simonds, J. H. Levine, S. C. Bendall, D. K. Shenfeld, S. Krishnaswamy, G. P. Nolan, and D. Pe'er. 2013. viSNE enables visualization of high dimensional single-cell data and reveals phenotypic heterogeneity of leukemia. *Nat. Biotechnol.* 31: 545–552.
36. Van Gassen, S., B. Callebaut, M. J. Van Helden, B. N. Lambrecht, P. Demeester, T. Dhaene, and Y. Saeys. 2015. FlowSOM: using self-organizing maps for visualization and interpretation of cytometry data. *Cytometry A* 87: 636–645.
37. Kamimura, Y., and L. L. Lanier. 2015. Homeostatic control of memory cell progenitors in the natural killer cell lineage. *Cell Rep.* 10: 280–291.
38. Spits, H., J. H. Bernink, and L. Lanier. 2016. NK cells and type 1 innate lymphoid cells: partners in host defense. *Nat. Immunol.* 17: 758–764.
39. Weizman, O.-E., N. M. Adams, I. S. Schuster, C. Krishna, Y. Pritykin, C. Lau, M. A. Degli-Esposti, C. S. Leslie, J. C. Sun, and T. E. O'Sullivan. 2017. ILC1 confer early host protection at initial sites of viral infection. *Cell* 171: 795–808.e12.
40. Meininger, I., A. Carrasco, A. Rao, T. Soini, E. Kokkinou, and J. Mjösberg. 2020. Tissue-specific features of innate lymphoid cells. *Trends Immunol.* 41: 902–917.
41. Huntington, N. D., H. Tabarias, K. Fairfax, J. Brady, Y. Hayakawa, M. A. Degli-Esposti, M. J. Smyth, D. M. Tarlinton, and S. L. Nutt. 2007. NK cell maturation and peripheral homeostasis is associated with KLRG1 up-regulation. *J. Immunol.* 178: 4764–4770.
42. Chiossone, L., J. Chaix, N. Fuseri, C. Roth, E. Vivier, and T. Walzer. 2009. Maturation of mouse NK cells is a 4-stage developmental program. *Blood* 113: 5488–5496.
43. Min-Oo, G., and L. L. Lanier. 2014. Cytomegalovirus generates long-lived antigen-specific NK cells with diminished bystander activation to heterologous infection. *J. Exp. Med.* 211: 2669–2680.
44. Nabekura, T., and L. L. Lanier. 2016. Tracking the fate of antigen-specific versus cytokine-activated natural killer cells after cytomegalovirus infection. *J. Exp. Med.* 213: 2745–2758.
45. Rex, D. A. B., N. Agarwal, T. S. K. Prasad, R. K. Kandasamy, Y. Subbannayya, and S. M. Pinto. 2020. A comprehensive pathway map of IL-18-mediated signalling. *J. Cell Commun. Signal.* 14: 257–266.
46. Kalina, U., D. Kauschat, N. Koyama, H. Nuernberger, K. Ballas, S. Koschmieder, G. Bug, W.-K. Hofmann, D. Hoelzer, and O. G. Ottmann. 2000. IL-18 activates STAT3 in the natural killer cell line 92, augments cytotoxic activity, and mediates IFN-γ production by the stress kinase p38 and by the extracellular regulated kinases p44erk-1 and p42erk-21. *J. Immunol.* 165: 1307–1313.
47. Wight, A., A. B. Mahmoud, M. Scur, M. M. Tu, M. M. A. Rahim, S. Sad, and A. P. Makrigiannis. 2018. Critical role for the Ly49 family of class I MHC receptors in adaptive natural killer cell responses. *Proc. Natl. Acad. Sci. USA* 115: 11579–11584.
48. Forbes, C. A., A. A. Scalzo, M. A. Degli-Esposti, and J. D. Coudert. 2014. Ly49C-dependent control of MCMV infection by NK cells is cis-regulated by MHC class I molecules. *PLoS Pathog.* 10: e1004161.
49. Scarpellino, L., F. Oeschger, P. Guillaume, J. D. Coudert, F. Lévy, G. Leclercq, and W. Held. 2007. Interactions of Ly49 family receptors with MHC class I ligands in trans and cis. *J. Immunol.* 178: 1277–1284.
50. Negi, S., D. K. Das, S. Pahari, S. Nadeem, and J. N. Agrewala. 2019. Potential role of gut microbiota in induction and regulation of innate immune memory. *Front. Immunol.* 10: 2441.
51. Aguilar, O. A., R. Berry, M. M. A. Rahim, J. J. Reichel, B. Popović, M. Tanaka, Z. Fu, G. R. Balaji, T. N. H. Lau, M. M. Tu, et al. 2017. A viral immunoevasin controls innate immunity by targeting the prototypical natural killer cell receptor family. *Cell* 169: 58–71.e14.
52. Hwang, I., T. Zhang, J. M. Scott, A. R. Kim, T. Lee, T. Kakarla, A. Kim, J. B. Sunwoo, and S. Kim. 2012. Identification of human NK cells that are deficient for signaling adaptor FcRγ and specialized for antibody-dependent immune functions. *Int. Immunol.* 24: 793–802.
53. Zhang, T., J. M. Scott, I. Hwang, and S. Kim. 2013. Cutting edge: antibody-dependent memory-like NK cells distinguished by FcRγ deficiency. *J. Immunol.* 190: 1402–1406.
54. Doucey, M.-A., L. Scarpellino, J. Zimmer, P. Guillaume, I. F. Luescher, C. Bron, and W. Held. 2004. Cis association of Ly49A with MHC class I restricts natural killer cell inhibition. *Nat. Immunol.* 5: 328–336.
55. Nabekura, T., M. Kanaya, A. Shibuya, G. Fu, N. R. J. Gascoigne, and L. L. Lanier. 2014. Costimulatory molecule DNAM-1 is essential for optimal differentiation of memory natural killer cells during mouse cytomegalovirus infection. *Immunity* 40: 225–234.
56. Mitrović, M., J. Arapović, S. Jordan, N. Fodil-Cornu, S. Ebert, S. M. Vidal, A. Krmpotić, M. J. Reddehase, and S. Jonjić. 2012. The NK cell response to mouse cytomegalovirus infection affects the level and kinetics of the early CD8(+) T-cell response. *J. Virol.* 86: 2165–2175.
57. Abel, A. M., C. Yang, M. S. Thakar, and S. Malarkannan. 2018. Natural killer cells: development, maturation, and clinical utilization. *Front. Immunol.* 9: 1869.
58. Madera, S., M. Rapp, M. A. Firth, J. N. Beilke, L. L. Lanier, and J. C. Sun. 2016. Type I IFN promotes NK cell expansion during viral infection by protecting NK cells against fratricide. *J. Exp. Med.* 213: 225–233.
59. Marcenaro, E., S. Carlomagno, S. Pesce, A. Moretta, and S. Sivori. 2011. NK/DC crosstalk in anti-viral response. *Adv. Exp. Med. Biol.* 946: 295–308.
60. Strauss-Albee, D. M., J. Fukuyama, E. C. Liang, Y. Yao, J. A. Jarrell, A. L. Drake, J. Kinuthia, R. R. Montgomery, G. John-Stewart, S. Holmes, and C. A. Blish. 2015. Human NK cell repertoire diversity reflects immune experience and correlates with viral susceptibility. *Sci. Transl. Med.* 7: 297ra115.
61. Joncker, N. T., N. C. Fernandez, E. Treiner, E. Vivier, and D. H. Raulet. 2009. NK cell responsiveness is tuned commensurate with the number of inhibitory receptors for self-MHC class I: the rheostat model. *J. Immunol.* 182: 4572–4580.
62. Brodin, P., T. Lakshmikanth, S. Johansson, K. Kärre, and P. Höglund. 2009. The strength of inhibitory input during education quantitatively tunes the functional responsiveness of individual natural killer cells. *Blood* 113: 2434–2441.
63. Sungur, C. M., Y. J. Tang-Feldman, E. Ames, M. Alvarez, M. Chen, D. L. Longo, C. Pomeroy, and W. J. Murphy. 2013. Murine natural killer cell licensing and regulation by T regulatory cells in viral responses. *Proc. Natl. Acad. Sci. USA* 110: 7401–7406.
64. Orr, M. T., J. C. Sun, D. G. T. Hesslein, H. Arase, J. H. Phillips, T. Takai, and L. L. Lanier. 2009. Ly49H signaling through DAP10 is essential for optimal natural killer cell responses to mouse cytomegalovirus infection. *J. Exp. Med.* 206: 807–817.
65. Kielczewska, A., M. Pyzik, T. Sun, A. Krmpotic, M. B. Lodoen, M. W. Munks, M. Babic, A. B. Hill, U. H. Koszinowski, S. Jonjic, et al. 2009. Ly49P recognition of cytomegalovirus-infected cells expressing H2-Dk and CMV-encoded m04 correlates with the NK cell antiviral response. *J. Exp. Med.* 206: 515–523.
66. Schenkel, A. R., L. C. Kingry, and R. A. Slayden. 2013. The ly49 gene family. A brief guide to the nomenclature, genetics, and role in intracellular infection. *Front. Immunol.* 4: 90.
67. Bergman, I., P. H. Basse, M. A. Barmada, J. A. Griffin, and N.-K. V. Cheung. 2000. Comparison of in vitro antibody-targeted cytotoxicity using mouse, rat and human effectors. *Cancer Immunol. Immunother.* 49: 259–266.